BOSTON UNIVERSITY

GRADUATE SCHOOL OF ARTS AND SCIENCES

Dissertation

KINETIC LATTICE MONTE CARLO AND AB INITIO STUDY OF POINT DEFECT MEDIATED DIFFUSION OF DOPANTS IN SILICON

by

MARIUS M. BUNEA

M.S. Bucharest University, 1991

Submitted in partial fulfillment of the

requirements for the degree of

Doctor of Philosophy

2000

Approved by

First Reader   _____

Scott T. Dunham
Associate Professor of Electrical Engineering

Second Reader   _____

Karl Ludwig
Associate Professor of Physics

Acknowledgments

I wish to thank my primary advisor Professor Scott T. Dunham for his boldness, direction and support in my doctoral work at Boston University. He also introduced me to the American life and gave me the first lesson in sailing. Professor Karl F. Ludwig guidance and encouragements were a great help in my last year of graduate studies. I would like to thank my committee members Professors Karl Ludwig, Steven Ahlen, Roscoe Giles and Sidney Redner for their constructive comments related to my research. Many thanks also go to Wolfgang Windl and Roland Stumpf, from Computational Material Group, Motorola Inc., that made ab-initio study of dopant diffusion in silicon a very rewarding and illuminating experience for me. My colleagues in process modeling group Mitra Navi, Alp Ghencer, Srinivasan Chakravarti, Pavel Fastenko, Brendon Murphy have been good friends and have given me a great deal of support.

I would like to acknowledge the Semiconductor Research Corporation whose financial support made this research project possible.

My special thanks go to my wife with whom in the eight years since we have been married did all the required work for our PhDs.

Lastly I would like to express my love and gratitude to my parents that kept me focused and cultivated in me the curiosity for other cultures and horizons, to my brother Carmen for his funny attitude toward life and constant encouragements. Without their love and support I would have never written this thesis.

KINETIC LATTICE MONTE CARLO AND AB INITIO STUDY OF POINT DEFECT MEDIATED DIFFUSION OF DOPANTS IN SILICON

(Order No.   )

MARIUS M. BUNEA

Boston University Graduate School of Arts and Sciences, 2000

Major Professor: Scott T. Dunham, Associate Professor of Electrical Engineering

ABSTRACT

Dopant diffusion in silicon has been studied for many years because of its importance in establishing dopant profiles in very large scale integrated devices, and because it is more complicated than would be predicted by Fick's law. As electronic devices become smaller and smaller, understanding the atomistic mechanisms for dopant diffusion becomes crucial for the continued rapid advance in technologies.

In this work, dopant diffusion in silicon is studied using kinetic lattice Monte Carlo (KLMC) and ab-initio calculations. The KLMC approach is used to span the time and length scales between microscopic and macroscopic diffusion regimes. A model based on a lattice occupied by different particles (dopants, vacancies, interstitials, silicon atoms) with medium range interactions (up to tenth nearest neighbor) is employed with a range of boundary conditions. Hopping rates are based on changes in system energy and satisfy detailed balance. Different diffusion mechanisms (e.g., ring, kick-out) are implemented. KLMC parameters (e.g., interactions energies) are obtained from both experiment as well as ab-initio and empirical potential MD calculations.

Problems investigated include: anomalous dopant diffusion in heavily doped silicon, corrections to continuum models for defect mediated dopant diffusion, damage annealing following ion implantation, boron diffusion in silicon. A computer program LAMOCA has been written to investigate these phenomena.

Contents

List of Figures

List of Tables

Chapter 1

Introduction

Dopant diffusion in silicon has been studied for many years because of its major technological importance as an elementary process step in fabrication of silicon based integrated circuits. Dopants atoms are introduced into silicon substrates with the purpose of changing the electrical conductivity of the host material. These dopants then diffuse during some of the subsequent steps required to make electronic devices. Diffusion of dopants in silicon is more complicated than predicted by Fick's law, and for the last 30 years continuum models, based on solving coupled diffusion equations for dopants and point defects, have been the standard approach. Although computationally fast, they have become very complex and as such their predictions are uncertain.

Due to significant improvements in computer power and computational methods in last decades a new field has emerged between the traditional experimental and theoretical physics which is computational physics or computer simulation[10].

The information provided by analitic theories is exact only in rare cases and for other cases uncertain approximations are required. For instance statistical problems which are solvable for three dimensional geometry are idealized cases like coupled

1

harmonic oscillators or ideal gases or ideal solutions.

Experiments on the other hand are almost never precisely characterized since the chemical constitution of a sample is known only approximatly. And in this way computer simulation could fill the gap between theory and experiment by testing if the model correctly represent the real system or not.

A new trend is emerging in the study of dopant diffusion in silicon which consists in using experimental results and a broad range of numerical methods (e.g., first principle calculations, molecular dynamics, kinetic lattice Monte Carlo, coupled diffusion equations) to gain insight into the interactions of dopants with point defects.

In this work, dopant diffusion in silicon will be studied using kinetic lattice Monte Carlo (KLMC) and ab-initio calculations. The KLMC approach is used to span the time and length scales between microscopic and macroscopic regimes. A lattice model with different particles (dopants, vacancies, interstitials, silicon atoms) with medium range interactions (up to tenth nearest neighbor) is employed with a range of boundary conditions. Hopping rates are based on changes in system energy and satisfy detailed balance. Different diffusion mechanisms (e.g., ring, kick out) are implemented. KLMC parameters (e.g., interactions energies) are obtained from both experiment as well as from ab-initio and empirical-potential MD calculations.

Chapter 2

Background

2.1 Point Defect Properties

2.1.1 Definition of Point Defects

Perfect crystals can be regarded as made of identical building blocks, unit cells, stacked in a repetitive array that defines the translational symmetry of the crystal structure. The crystal surface destroys the symmetry of the crystal. Its effects are neglected by definition in the study of bulk properties. While other extended defects are present in the crystal, point defects are of principal interest from the perspective of dopant diffusion in silicon. Two types of point defects may be identified: impurities and thermally activated point defects. Impurities are incorporated in silicon crystals from the growth process or in subsequent steps meant to introduce dopants that upon activation will change the electrical properties of silicon. Thermally activated point defects or native point defects are present in the equilibrium structure of crystals at non-zero temperatures. Atomic motion associated with thermal energy causes atomic coordinates to fluctuate about their time average values and may have the effect of displacing the atoms from lattice sites into interstices where they may find

new equilibrium positions as *interstitial* atoms. The empty site left behind when an interstitial is created is called *vacancy* (see Fig. 2.1. This defect is also called a Schotcky defect. A vacancy can exist in different charged states V^+, V^{++}, V^0, V^-, V^{--} (see Watkins *et al.[1]* for a complete study of vacancy in different charged states). For every charged state, the lattice presents a different distortion. These local distorsions will be ignored in the lattice model that will be used to study diffusion. Only for a vacancy in the neighborhood of a dopant they are accounted for indirectly via the dopant-vacancy interaction potential. An interstitial is an atom transferred from a lattoce site to a position not occupied by an atom in a perfect crystal. An interstitialcy is a defect which consists of two atoms sharing a lattice site. A dopant

Vacancy   Interstitial   Interstitialcy
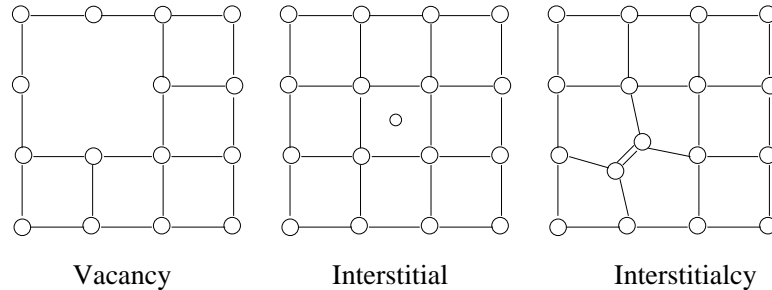
Figure 2.1: Native point defects of interest for silicon: vacancy - an empty lattice site, interstitial - an atom transfered from a lattice site to a position not occupied by an atom in the perfect crystal, and interstitialcy - two atoms sharing a site.

atom which resides on a lattice site is called a substitutional defect.

2.1.2   Why Study Point Defects ?

Dopant atoms dissolve substitutionally in silicon. It was assumed that only by interacting with point defects, vacancies and interstitials, dopant atoms will performe long range diffusion. Although the importance of the vacancy and interstitial mechanism on dopant diffusion is still debated experiments suggest that P and B have the most

substantial interstitial component on diffusion, while Sb appears dominated by a vacancy mechanism. Oxidation of a silicon surface above an impurity doped layer leads to a large increase in the impurity diffusion above what is normally observed[2, 3]. At the same time extended defects - stacking faults grow (see Fig. 2.2. TEM obser-
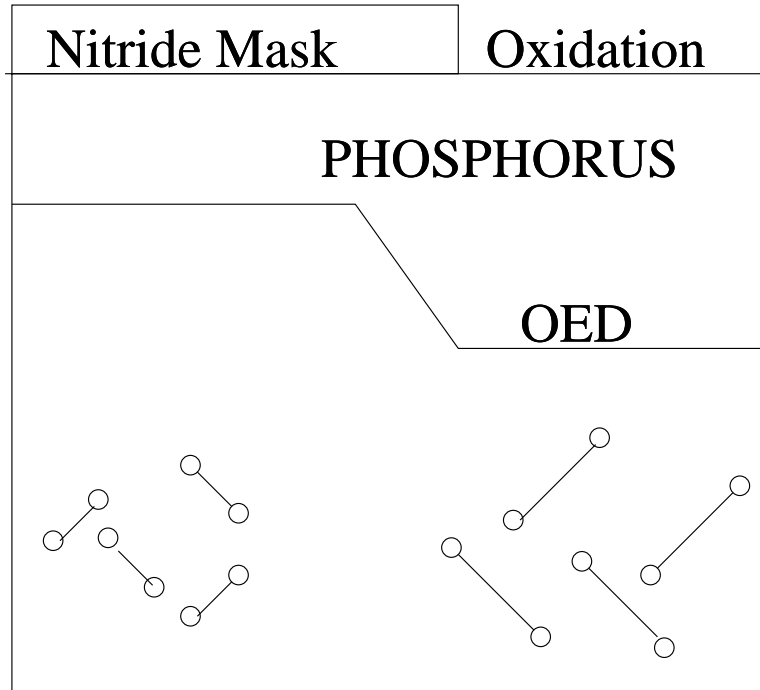
Figure 2.2: A schematic picture that shows the enhanced diffusion of phosphorous under the oxidazing region and the growth of stacking faults. Hu[4] proposed that the two phenomena have a common origin in the injection of silicon self interstitials. This type of experiment suggests that difussion of impurities like P and B are dominated by an interstitial mechanism.

vation of stacking faults show that they were interstitial type defects. It was known that these defects grow by adding silicon atoms to the dislocation ends in oxidizing ambients. Hu[4] linked the growth of stacking faults and oxidation enhanced diffusion of dopants by proposing that they are due to silicon interstitials injected during oxidation. Under the same conditions antimony diffusion is retarded which is explained

trough decrease in the vacancy concentration due to the excess of interstitials and is evidence for a dominating vacancy mechanism for antimony diffusion.

2.1.3   Thermodynamics of Point Defects

Why do point defects exist ? Usually silicon wafers are kept at constant temperature and pressure. Under these conditions the thermodynamical potential that is minimum at equilibrium is the Gibbs free energy:

$$G = H - TS \qquad (2.1)$$

where H is the enthalpy, T is the absolute temperature, S is the entropy. At any non-zero temperature the silicon crystal will have a finite concentration of point defects, due to the fact that the energy cost for formation of a point defect is compensated by the entropy contribution and in this way the presence of point defects minimizes the free energy. Upon formation of a defect X (interstitial or vacancy) the change in the free energy is:

$$\Delta G_X = \Delta H_X^f - T\Delta S_X \qquad (2.2)$$

ΔH_X^f is the enthalpy required to form a point defect X. The total entropy is the sum of three terms:

$$\Delta S_X = \Delta S_X^m + \Delta S_X^c + \Delta S_X^f \qquad (2.3)$$

(mixing, configuration and formation entropies). The entropy of mixing depends on the number of different possible arrangements of point defects within the crystal and is defined as the difference in the entropy associated with the presence of n_X point

defects versus n_{X-1}.

$$\Delta S_X^m = k\mathrm{ln}w(n_X) - k\mathrm{ln}w(n_X - 1) = k\mathrm{ln}[\frac{w(n_X)}{w(n_X - 1)}] \tag{2.4}$$

Where $w(n_X)$ is the number of different possible arrangements of vacancies within the crystal. The configuration entropy, which depends on the number of different configurations of the vacancy θ_X is just:

$$\Delta S_X^c = k\mathrm{ln}\theta_X \tag{2.5}$$

The remaining entropy change is called formation entropyΔS_X^f. At equilibrium $\Delta G_X = 0$ and substituting for the entropy terms we obtain:

$$\Delta H_X^f - T(\Delta S_X^m + \Delta S_X^c + \Delta S_X^f) = \Delta H_X^f - T\Delta S_X^f - kT\mathrm{ln}\left[\frac{\theta_X(C_s - C_X)}{C_X}\right] \tag{2.6}$$

After some rearrangements and in the limit of dilute solutions$(C_X \ll C_s)$ we obtain:

$$C_X^* \simeq \theta_X C_s \mathrm{exp}\left[-\frac{\Delta G_X^f}{kT}\right] = 0 \tag{2.7}$$

where $\Delta G_X^f = \Delta H_X^f - T\Delta S_X^f$, C_s is the concentration of sites and C_X is the concentration of defects.

2.1.4   Nature of the Dopant Defect Interaction Potential

For analysing dopant diffusion in silicon in the following chapters will be usefull to know how a dopant and a point defect interact. This interaction is described trough an interaction potential and is calculated using quantum mechanics via what is called first principle calculations which will be presented in the next chapter. There are two

main contributions to the dopant-point defect interaction: Coulombic and elastic. The dopant and the defect usually carry electric charge and as such a Coulombic potential between an ionized dopant atom and a charged point defect arises:

$$\Delta E_{Coul} = \frac{q_1 q_2}{4\pi \epsilon_0 \epsilon_{Si} r} \qquad (2.8)$$

where q_1 and q_2 are the charges on the two interacting particles, r the distance between them, and ϵ_{Si} is the macroscopic dielectric constant of Si (ϵ_{Si}=11.7). For close range interaction one performs more sofisticated corrections, Madelung like, in the previous equation. In Fig. 2.3 the dopant-vacancy interaction potential from Pankratov *et al.*[5] and Nelson *et al.*[6, 7] is shown for As and P. Some distortion of the lattice must occur in order to accomodate either native point defects or dopant atoms. Atoms with shorter bonding radii than silicon ($r_{Si} = 1.17\mathring{A}$) are said to be "smaller" than silicon. Such dopants are P and B ($r_P = 1.1\mathring{A}$, $r_B = 0.88\mathring{A}$). All other dopants(Al, Ga, In, As, Sb and Bi) are "larger" than silicon ($r_A = 1.26, 1.26, 1.44, 1.18, 1.36, 1.45\mathring{A}$ respectively. The size of the dopant atoms has a visible effect on the silicon lattice. Thus small atoms contract the lattice, big atoms dilate the silicon lattice. Nelson *et al.* have calculated the bond lenght for substitutional impurities and found that they follow the general trend of shorter bond lenghts with atomic size (see Table 2.1). The bond lenghts calculated are consistent with predictions based on a sum of covalent radii. The lattice relaxes inward for small atoms (B, C, N) and outward for big atoms (Al, Sb). As a result one finds smaller binding energy between a dopant with a inward relaxation and a vacancy, and a larger binding energy between a dopant and a vacancy.

Self diffusion and dopant diffusion, as will be discussed at large in the following
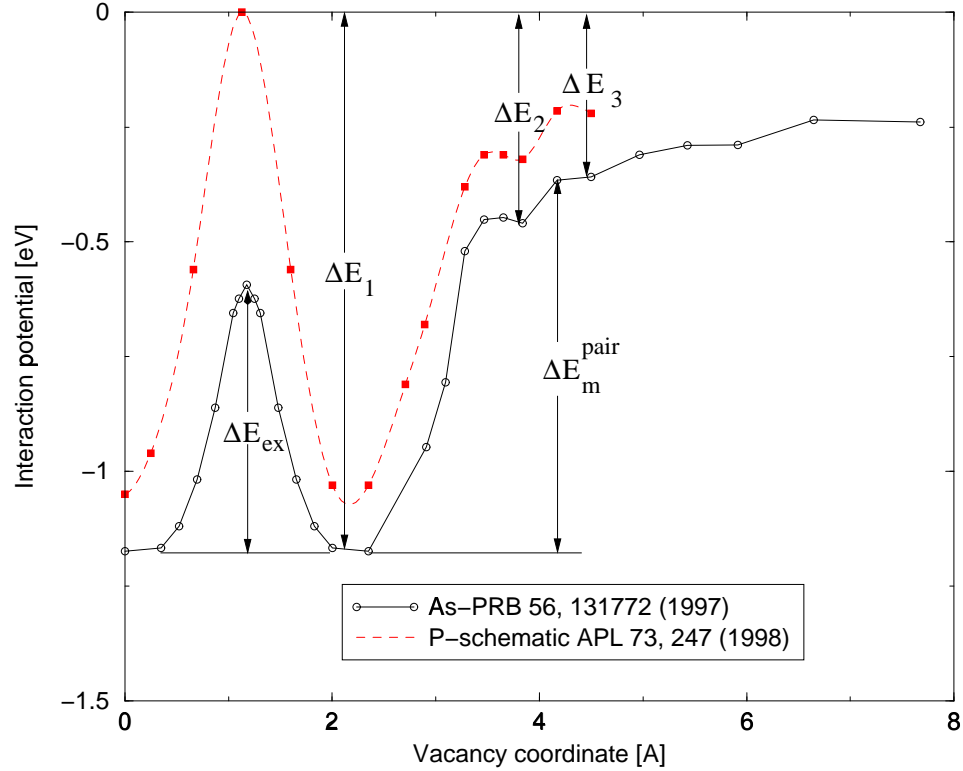
Figure 2.3: The As-vacancy and P-vacancy interaction potential. The dopant atom is placed in the origin of the horizontal axis. The numbers on the horizantal axis enumerate lattice sites relative to the dopant atom. ΔE_{ex} is the energy barrier for the As atom to hop in the empty site (dopant-vacancy exchange), ΔE_1, ΔE_2 and ΔE_3 are the binding energies for for the dopant-vacancy pair at first, second and third nearest neighbor, ΔE_m^{pair} is the migration barrier for the As-vacancy pair.

chapters, can be described by an Arrhenius expression:

$$d = d_0 \exp(-Q/kT) \tag{2.9}$$

Experiments[3] find the activation energy for dopant diffusion to be 1 eV or more lower than self-diffusion. If one mechanism is dominant over the other then the activation energy is written as a sum of the defect formation enthalpy H_X^f and defect

Table 2.1: Si impurity bond lenghts

Dopant	Calculated bond lenght	Sum of covalent radii
B	2.06	1.98
C	2.01	1.94
N	2.02	1.87
Al	2.39	2.42
Si	2.33	2.34
P	2.33	2.27
Sb	2.60	2.58

migration enthalpy H_X^m:

$$Q_u = H_X^f + H_X^m \tag{2.10}$$

2.2 Atomistic Models for Point Defect Mediated Diffusion

2.2.1 Vacancy Mechanism

One way a substitutional dopant can diffuse through the lattice is by moving onto an adjacent vacant site. A schematic of this process is shown in Fig. 2.4. This diffusion mechanism has been proposed for silicon based on the experimental observation that vacancy is the main point defect in metals[8]. At an atomistic scale this mechanism presents some particularities given the different dopant-vacancy interactions. For As for instance, the vacancy mechanism does not occur through just a simple dopant vacancy exchange, but through what is called "ring mechanism". The vacancy not only is exchanging its position with the dopant but has to reach the third nearest neighbor with respect to the dopant and approach the dopant from a new direction for a long range migration of the dopant to take place. This mechanism is possible given the energy barriers associated with silicon or dopants atom hops onto the empty
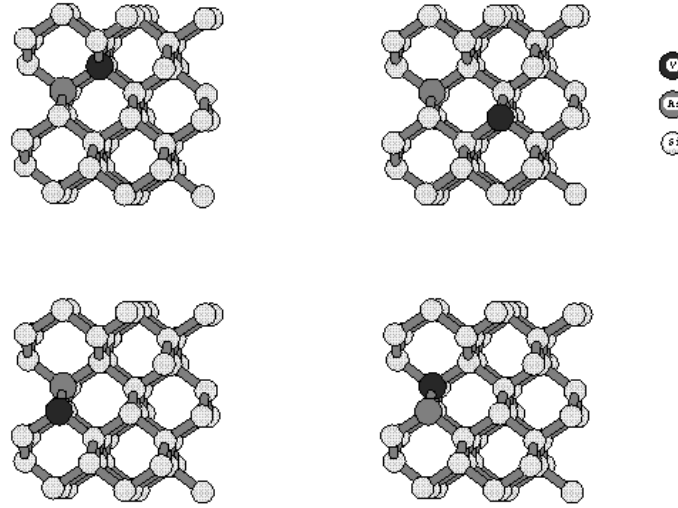
Figure 2.4: The dopant vacancy pair migration on the silicon lattice. The empty site (vacancy) is shown as a dark particle to explain the mechanism better. In the upper left figure the dopant and the vacancy are first nearest neighbors. The hopping rates are such that the dopant can hop into the empty site and backwards many times (a phenomenon 'called' caging in metals) without any effect on diffusion. The host atoms though could hop into the empty site such that at some point the vacancy can be located as third nearest neighbor with respect to the dopant as in the upper right figure. Then the vacancy can go around the six member ring of atoms and approach the dopant from a different direction as in the lower left figure. In metals this is called looping. Following another hop of the dopant into the empty site, as in the lower right figure, the dopant makes one relevant step for diffusion. The dopant vacancy pair has performed one step as a random walker. The ring mechanism for diffusion is such a combination of dopant-vacancy interaction and geomtry of silicon structure.

sites that are calculated by quantum mechanics via first principle calculations.

The activation energy is usually written for dopant diffusion as the sum of the pair formation energy H_{AV}^f and and the pair migration energy H_{AV}^m.

$$Q = H_{AV}^f + H_{AV}^m \tag{2.11}$$
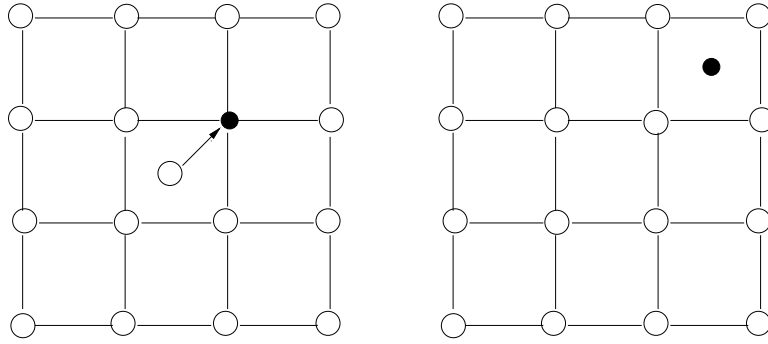
Figure 2.5: Dopant diffusion via interstitial mechanism. The dark atom is an substitutional dopant. A silicon self interstitial hopping through the interstices of the silicon lattice approaches the substitutional dopant and the energy barrier is low enough that the dopant is kicked out of its site into an interstices and then could migrate through the interstices of the Si lattice until kikcs out a host atom and becomes substitutional again.

where the formation enthalpy of the pair $H^f_{AV} = H^f_V - E^b_{AV}$ and E^b_{AV} is the binding energy of the AV pair. For other dopants like P the limiting step is not the vacancy reaching the third nearest neighbor site with respect to the dopant but dopant vacancy exchange.

2.2.2   Interstitial Mechanism

In this mechanism a silicon interstitial migrates trough the interstices of the lattice and approaches a substitutional atom. If the energy barrier is low, the substitutional dopant becomes an interstitial atom and could migrate through the lattice as a dopant interstitial. This process is described by the reaction:

$$A_s + I \Leftrightarrow A_i, \tag{2.12}$$

An example of the interstitial mechanism is shown in Fig. 2.5.

Chapter 3

Numerical Methods Employed

3.1 Kinetic Lattice Monte Carlo

3.1.1 Statistical Mechanics of KLMC

In the lattice model where KLMC will be used it is assumed that atoms oscillate with small amplitudes about fixed sites, at high temperatures ar which diffusion usually takes place, and now and then hop to empty sites if such sites are first nearest neighbors. The classical hamiltonian contains a kinetic and a potential term [**?**]:

$$H(\vec{p}, \vec{r}) = T(\vec{p}) + V(\vec{r}) \tag{3.1}$$

such that the probability density of finding the system in the neighborhood of a phase space point $(\vec{p}, \vec{r})$ is :

$$P(\vec{p}, \vec{r}) = \frac{1}{Z}\exp(-\beta H(\vec{p}, \vec{r})), \tag{3.2}$$

where $\beta = 1/k_B T$, k_B is Boltzmann's constant and T is the absolute temperature. Z is the partition function and has the value:

$$Z = \int d\vec{p} \int d\vec{p} \, \exp(-\beta H(\vec{p}, \vec{r})) \qquad (3.3)$$

In Monte Carlo method the momenta of the atoms are neglected. Integrating over momenta one obtains the probability density of having the system in the neighborhood of some set of spatial coordinates:

$$P(\vec{r}) = 1/Q \exp(-\beta V(\vec{r})) \qquad (3.4)$$

Now we introduce the harmonic approximation for the potential energy $V(\vec{r})$. The set of sites about which atoms vibrate are $\vec{R_i}$ for some configuration i. When the atoms occupy these sites the local energy is minimum and the atoms experience no force. If the net displacements from these sites is given by $\vec{u}$, $\vec{r} = \vec{R_i} + \vec{u}$. Within the harmonic approximation the potential energy can be written as:

$$V(\vec{r}) \approx V(\vec{R_i}) + \frac{1}{2} \vec{u} \, \mathbf{D_i} \, \vec{u} \qquad (3.5)$$

The integral over $\vec{r}$ is replaced with a sum over i and and integral over $\vec{u}$. Assuming that the dynamical matrix is independent of configuration and integrating over $\vec{u}$ we get the probability of the system to be in the configuration i.

$$P(\vec{R_i}) = \frac{\exp(-\beta V(\vec{R_i}))}{\sum_j \exp - \beta V(\vec{R_j})} \qquad (3.6)$$

3.1.2   Kinetics of KLMC

Transition from one state to another is governed by the Markovian master equation:

$$\frac{\partial P_i}{\partial t} = -P_i W_{ij} + \sum_j P_j W_{ji} \tag{3.7}$$

where P_i is the probability of finding the system in a state i, W_{ij} is the rate of going from a state i into another state j. At local equilibrium detailed balance holds:

$$P_i W_{ij} = P_j W_{ji} \tag{3.8}$$

Combining equations (3.4) and (3.8) we obtain:

$$\frac{W_{ij}}{W_{ji}} = \exp(-\beta V(\vec{R}_j) - V(\vec{R}_i)) \tag{3.9}$$

The transition rates from one state to another could be postulated or taken from transition state theory (TST):

$$W_{ij} = W_0 \exp\left(-\frac{\beta}{2}\left[V(\vec{R}_j) - V(\vec{R}_i)\right]\right) \tag{3.10}$$

where W_0 corresponds to the attempt frequency of crossing the barrier from one state to another.

To obtain equation (3.10) other theories could be used like lattice gas theory applied to a binary alloy[11] where the lattice is populated with different types of atoms, say 1 and 2, numbering N_1 and N_2, with the numbers of nearest neighbors being N_{11}, N_{22}, N_{12} such that the configuration energy could be written as:

$$E = \epsilon_{11} N_{11} + \epsilon_{22} N_{22} + \epsilon_{12} N_{12} \tag{3.11}$$

where ϵ_{11}, ϵ_{22} and ϵ_{12} denote the interaction energies of the different types of pairs.

The number of particles could be kept constant as in Kawasaki models, or could change during the evolution of the system like in Glauber models.

The time is defined such that the diffusivity of an individual vacancy matches the value predicted from molecular dynamics calculations[12].

Note also that in a the KLMC method because the momenta of atoms are neglected time is artificial.

Diffusion is by its nature a nonequilibrium phenomenon. In our case we will use a latice model where each site is either empty or occupied by a host atom or a dopant atom. The vacant site will be treated for simplication as another species. The dopant atoms that occupy interstitial sites can also hop with hopping rates that will be postulated.

3.2   Ab-initio Pseudopotential Calculations

3.2.1   Introduction in Pseudopotential Method

In solving the Schrödinger equation for solids, space can be divided into two regions with quite different properties. The regions near nuclei, the "core regions", are composed of tightly bound electrons which respond very little to the presence of neighboring atoms, while the remaining volume contains the valence electrons density which are involved in the bonding together of the atoms. Although the potential in the core is strongly attractive for valence electrons, the requirement that valence electrons be orthogonal to those of the core produces a large kinetic energy which contributes an effective repulsive potential for the valence states. The valence electrons are responsible for the main properties of solids. To find the eigenstates and

eigenvalues of these valence electrons one needs to solve the Schrödinger equation with some boundary conditions at the core radius r_c.

We obtain the same valence eigenfunctions and eigenvalues if we work with a 'pseudopotential'(which inside the core is very weak and produces a nodeles 'pseudofunction') identical with the real potential outside the core, as long as the "pseudofunction" produces the same boundary condition as the real eigenfunction. In this way the valence electrons 'do not know' that something was changed in the core region. But we have now a weak pseudopotential that can be treated by the perturbation theory.

The pseudopotential approach represents a major achievement in band structure calculation. Usually in band structure calculation one deals with difficult questions related to self-consistent crystal potentials which very often obscure the underlying physical features.

By contrast the pseudopotential method avoids these difficulties at very little, if any, cost in acccuracy.

One area of application for pseudopotential method is the study of energetics of point defects.

The pseudopotential method grew out of the orthogonalized plane wave (OPW) method, in which wave functions were expanded in a set of plane waves (PW) which are orthogonalized to all of the core wavefunctions $|\Psi_c\rangle$:

$$|\text{OPW},K\rangle = |\text{PW},K\rangle - \sum_c^{core} |\Psi_c\rangle\langle\Psi_c|\text{PW},K\rangle \qquad (3.12)$$

where the wavevector K labels the PW or OPW.

The construction of a pseudopotential can be demonstrated in terms of the exact

core and valence states $|\Psi_c\rangle$, $|\Psi_v\rangle$, which satisfy:

$$H|\Psi_i\rangle = E_i|\Psi_i\rangle, \qquad i = \text{c,v} \tag{3.13}$$

We can substract the core orthogonality wiggles to obtain the pseudostates $|\Phi_v\rangle$ given by:

$$|\Phi_v\rangle = |\Psi_v\rangle + \sum_c |\Psi_c\rangle \alpha_{cv} \tag{3.14}$$

with $\alpha_{cv} = \langle\Psi_c|\Phi_v\rangle$. Applying H to $|\Phi_v\rangle$ gives:

$$H|\Phi_v\rangle = E_v|\Psi_v\rangle + \sum_c E_c|\Psi_c\rangle\alpha_{cv} = E_v|\Phi_v\rangle + \sum_c (E_c - E_v)|\Psi_c\rangle\alpha_{cv} \tag{3.15}$$

or

$$\left\{ H + \sum_c (E_v - E_c)|\Psi_c\rangle\langle\Psi_c| \right\} |\Phi_v\rangle = E_v|\phi_v\rangle \tag{3.16}$$

Thus the valence pseudostates $|\Phi_v\rangle$ satisfy a Schrödinger equation with an energy-dependent pseudo-Hamiltonian:

$$H^{ps}(E) = H + \sum_c (E - E_c)|\Psi_c\rangle\langle\Psi_c| \tag{3.17}$$

3.2.2 Density Functional Theory

A periodic system is considered with atoms at positions $\mathbf{R} + \tau$,where $\mathbf{R}$ is a Bravais lattice vector locating a unit cell of the crystal and τ is a basis vector giving the positions in the unit cell. The Hamiltonian of the system is given by:

$$H = -\sum_{i=1}^{N} \frac{1}{2m}\nabla_i^2 + \sum_{i=1}^{N} V_{ion}(\mathbf{r_i}) + \frac{1}{2}\sum_{i\neq j}^{N} v(\mathbf{r_i} - \mathbf{r_j}) + V_{I-I} \tag{3.18}$$

which describes N electrons at positions $\mathbf{r_i}$ interacting via the Coulomb potential $v(\mathbf{r}) = e^2/|\mathbf{r}|$ and moving in the potential of the static ions given by:

$$V_{ion}(\mathbf{r}) = \sum_{m,s} V_{ion}^{(s)}(\mathbf{r} - \mathbf{R_m} - \tau_{\mathbf{s}}) \tag{3.19}$$

The ion ion repulsion is given by:

$$V_{I-I} = \frac{1}{2} \sum_{mm'ss'}^{'} \frac{Z_s Z_{s'} e^2}{|\mathbf{R_m} + \tau_{\mathbf{s}} - \mathbf{R_{m'}} - \tau_{\mathbf{s'}}|} \tag{3.20}$$

where the $m = m'$, $s = s'$ is to be omitted from the summation. I will use in this report Rydberg atomic units $\hbar = 1$, $2m = 1$, $e^2 = 2$, distances beeing measured in Bohr and energies in Rydbergs. The first three terms in eq. 3.18 could be lumped together as the electron energy operator H^{el}. A central result in DFT is that the ground state electronic energy E^{el} of the system is given by:

$$E^{el} = T_0[n] + \int V_{ion}(\mathbf{r})n(\mathbf{r})\mathrm{d}\mathbf{r} + E_h[n] + +E_{xc}[n] \tag{3.21}$$

where $T_0[n]$ is the kinetic energy of a system of non-interacting electrons with density $n(\mathbf{r})$, E_h is the classical interaction energy:

$$E_h(n) = \frac{1}{2} \int \int n(\mathbf{r})v(\mathbf{r} - \mathbf{r'})n(\mathbf{r'})\mathrm{d}\mathbf{r}\mathrm{d}\mathbf{r'} \tag{3.22}$$

and E_{xc} is the exchange-correlation energy, which is a functional of n.

Then E_{el} is minimized with respect to density:

$$\left. \frac{\delta E^{el}[n]}{\delta n(\mathbf{r})} \right|_{n=n_0} = \mu \tag{3.23}$$

where μ is the chemical potential of the electronics system.

The last equation is satisfied if the following set of the Kohn-Sham equations is solved self-consistently:

$$h\Psi_i(\mathbf{r}) = \left\{ -\frac{1}{2m}\nabla^2 + V_{eff}(\mathbf{r};n) \right\} \Psi_i(\mathbf{r}) = \epsilon_i \Psi_i(\mathbf{r}) \tag{3.24}$$

$$V_{eff}(\mathbf{r};n) = V_{ion}(\mathbf{r}) + V_h(\mathbf{r};n) + V_{xc}(\mathbf{r};n) \tag{3.25}$$

$$n(\mathbf{r}) = \sum_{i=1}^{N} |\Psi_i(\mathbf{r})|^2 \tag{3.26}$$

Here $\{\Psi_i\}$ and $\{\epsilon_i\}$ are the orthonormal eigenfunctions and the eigenvalues of the one-electron Hamiltonian h. The Hartree and exchange-correlation (XC) potentials are given by:

$$V_h(\mathbf{r};n) = \int v(\mathbf{r} - \mathbf{r}\prime)n(\mathbf{r}\prime)\mathrm{d}\mathbf{r}\prime \tag{3.27}$$

$$V_{xc}(\mathbf{r};n) = \frac{\delta Exc[n]}{\delta n(\mathbf{r})} \tag{3.28}$$

Ψ_i and ϵ_i resemble the excited wavefunctions and energies of the many body systems.

3.3 Local Density Approximation

The success of the density functional theory would not have bee possible if not for an approximation related to the exchange-correlation of the electronic system called local density approximation. In thia approximation it is assumed that the exchange-correlation energy per electron at point $\mathbf{r}$ in the electron gas $\epsilon_{XC}(\mathbf{r})$ is the same to exchange-correlation energy per electron in a homogeneous electron gas that has the

same density as the electron gas at point $\mathbf{r}$.

$$E_{XC}[n(\mathbf{r})] = \int \epsilon_{XC}(\mathbf{r})n(\mathbf{r})d\mathbf{r} \qquad (3.29)$$

with

$$\epsilon_{XC}(\mathbf{r})\epsilon_{XC}^{hom}[n(\mathbf{r})] \qquad (3.30)$$

3.4   Nudged Elastic Band Method

An important problem in diffusion processes in solids is the identification of the lowest energy path for a rearrangement of a group of atoms from one stable configuration to another[?]. The potential energy maximum along such a path is the saddle point energy which gives the activation energy barrier, a quantity of central importance in our kinetic lattice Monte Carlo studies of impurity diffusion in silicon.

Widely used methods for finding reaction paths and saddle points make use of two point boundary condition, where both the initial and the final configurations for the transition are given.

They are usually two local minima on the multidimensional potential energy surface which may be obtained by Monte Carlo simulated annealing methods or molecular dynamics. A chain of states (or images) of the system is generated between the end point configurations and all the intermediate images are optimized simultaneously.

In the so called 'chain of states methods' several images are connected together to form a path and a function, called object fubnction is minimized with respect to the intermadiate images to find the lowest energy path. One example of such a function

in the space of configurations connected via springs is:

$$S(\vec{R_1}, \vec{R_2} \, ... \, \vec{R_{P-1}}) = \sum_{i=0}^{P} V(\vec{R_i}) + \sum_{i=1}^{P} \frac{Pk}{2}(\vec{R_i} - \vec{R_{i-1}}) \qquad (3.31)$$

where $V(\vec{R_i})$ is a potential function associated with a given configuration, the socond term in the above parameter is the elastic energy associated to a spring connecting images i and j, k is a parameter which has the significance of a spring constant. The end points R_0 and R_P are kept fixed. This method is called the plain elastic method.

There are usually two problems with the plain elastic method. The force acting on image i is:

$$\vec{F_i} = -\vec{\nabla} \, V(\vec{R_i}) + \vec{F_i^s} \qquad (3.32)$$

where

$$\vec{F_i^s} = k_{i+1}(\vec{R_{i+1}} - \vec{R_i}) - k_i(\vec{R_i} - \vec{R_{i-1}}) \qquad (3.33)$$

For a bigger value of k (e.g. k=1) the elastic band is too stiff and cuts the corner and misses the saddle point. For a smaller value of k (e.g. k=0.1) the images slide down and avoid the barrier region, reducing the resolution of the path in the critical region. The solution to the above problems in nudged elastic band method is to project out the perpendicular component of the spring force and the parallel component of the true force, such that the force on image i becomes:

$$\vec{F_i^0} = -\vec{\nabla} \, V(\vec{R_i})|_\perp + \vec{F_i^s} \, \dot{\tau}_\| \tau_\| \qquad (3.34)$$

where $\tau_\|$ is the unit tangent to the path.

Chapter 4

Corrections to Continuum Models

4.1   Corrections to pair diffusion model

A central question in understanding dopant diffusion is how to relate the macroscopic diffusion behavior to the microscopic processes involving interactions between individual particles. For a strong dopant-vacancy binding energy, as shown in Fig. 2.2, migration of dopant-vacancy pairs occurs. The "pair diffusion" model[16, 17], as also described by Eq. 2.11, is currently the standard approach used in continuum simulators [3]. Previous work[15] studied the validity of this model and that of an alternative "non Fickian diffusion" model[18, 19] by taking into account a variety of assumed dopant-vacancy interaction potentials. It was found that for an attractive potential the dopant flux is in the same direction as the vacancy flux, and is dependent on the difference between activation energy of the dopant diffusivity and that of tracer diffusion.

In this work the direction and the magnitude of a dopant flux in a vacancy gradient is studied for two substitutional dopants, As and P, related to their diffusion via a vacancy mechanism in silicon at moderate doping levels. A lattice model is used

with transition rates based on recent first-principle calculations [5, 6, 7] for dopant-vacancy interaction up to third nearest neighbor distance (4.5 Å) for P and sixth nearest neighbor (6.65 Å) for As. Results over a range of temperatures are compared to the pair diffusion model.

Two approaches can be used to relate the flux of dopants driven by a gradient of vacancies when a local thermodynamic equilibrium is assumed. In a first, more general approach[15, 20] following Onsager's[21] linearized nonequilibrium transport theory, the dopant flux is described by the following equation:

$$J_A = -\Lambda_{AA}\nabla\mu_A - \Lambda_{AV}\nabla\mu_V, \tag{4.1}$$

where Λ_{AA} and Λ_{AV} are the Onsager coefficients and μ_A, μ_V are the chemical potentials of dopants and vacancies. Writing the chemical potentials as functions of particle concentrations C_A, C_V for low concentrations one obtains:

$$J_A = -D_{AA}\nabla C_A - D_{AV}\nabla C_V, \tag{4.2}$$

where D_{AA} is the effective diffusion coefficient of dopant and D_{AV} accounts for the flux of dopant driven by a vacancy gradient.

A second approach, based on the pair diffusion model, finds a similar expression from Fick's first law and the mass action law ($C_{AV} = K_{AV}C_AC_V$) for the reaction of a substitutional dopant and a vacancy[16, 17]:

$$J_A = -K_{AV}d_{AV}[C_V\nabla C_A + C_A\nabla C_V], \tag{4.3}$$

where C_A and C_V are dopant and vacancy densities, and d_{AV} is the pair diffusivity. See Appendix A for proof.

This expression is widely used in process simulators[22]. To quantify the results of this work, Equation (3) is modified to include a correction factor γ:

$$J_A = -K_{AV}d_{AV}[C_V \nabla C_A + \gamma C_A \nabla C_V]. \tag{4.4}$$

Comparing Equations (2) and (4), $D_{AA} = K_{AV}d_{AV}C_V$ and $D_{AV} = \gamma K_{AV}d_{AV}C_A$.

In the pair diffusion model γ is assumed to be 1.

In this work, γ is calculated by performing kinetic lattice Monte Carlo (KLMC) simulations[23, 24, 25] with *ab-initio* dopant-vacancy interactions based on *ab-initio* results[5, 6, 7] (Table 4.1). The *ab-initio* method employed is described in references [4-6]. The dopant vacancy pair is treated as neutral, with the dopant in positively charged state and the vacancy in a negatively charged state, as is the case for moderately to heavily As or P doped silicon due to the linear dependence of the diffusivity on n/n_i, where n and n_i are the electron concentrations under extrinsic and intrinsinc doping conditions. Simulations were initiated by placing one dopant and one vacancy randomly on a silicon lattice. At each step the vacancy exchanges its site with a dopant atom or a silicon atom. Only hops to first nearest neighbor sites are considered. Transition rates satisfy detailed balance and are postulated to be:

$$\nu = \nu_m \exp\left[\frac{E_i - E_f}{2k_B T}\right], \tag{4.5}$$

where $E_i - E_f$ is the change in the system energy associated with a possible hop, k_B is Boltzmann's constant, and T is the absolute temperature. The correction factor γ is the same if different transition rates based on *ab-initio* saddle points[26] are used. At each step, time is incremented by the inverse of the sum of all transition rates.

For exchanges with silicon atoms, the value of ν_m associated with vacancy hops

Table 4.1: Exchange energy barrier and binding energies up to sixth nearest neighbor for As-vacancy and up to third nearest neighbor for P-vacancy from recent *ab-initio* calculations[5, 6, 7]. All energies are given in eV.

Dopant	E_{exch}	E_b^1	E_b^2	E_b^3	E_b^4	E_b^5	E_b^6
As	0.58	1.17	0.46	0.36	0.29	0.29	0.23
P	1.05	1.05	0.59	0.47			

is chosen such that the diffusivity of vacancies in pure silicon (D_v=0.125νa^2) is $D_v = 1.18 \times 10^{-4} \exp(-0.2\text{eV}/k_B T)$ cm^2/sec, where 0.2 eV is the migration enthalpy as obtained from *ab-initio* calculations[7] and the prefactor (which does not effect the calculation of the correction factor γ) is from tight binding molecular dynamics calculations[12]. Ab-initio calculations have an error of 0.1 eV for migration enthalpy and experimental values[1] are between 0.18 eV and 0.45 eV for vacancy in different charged states. 0.2 eV values has been used because it was obtained by the same method as the one that found the exchange and binding energies. Thus the parameters used are a self consistent set. Tests with migration enthalpy between 0.1 eV and 0.3 eV found the same value for the correction factor γ. For dopant-vacancy exchange, the migration enthalpy in ν_m is changed to match the calculated exchange barriers (Table 4.1). Note that a very large exchange barrier is calculated for P, such that P-V exchange, rather than separation to third-nearest neighbor distance is the rate limiting step for diffusion[25].

The vacancy gradient is implemented by adding a bias to vacancy transition rates between the bottom ($z = N_z - 1$) and top ($z = 0$) of the simulation cell.

$$\nu(1 \rightleftharpoons 2) = \nu \exp(\pm b) \tag{4.6}$$

Otherwise periodic boundary conditions are imposed. In Fig. 4.1 we see that the probability to find the vacancy on one of the (001) planes perpendicular to the
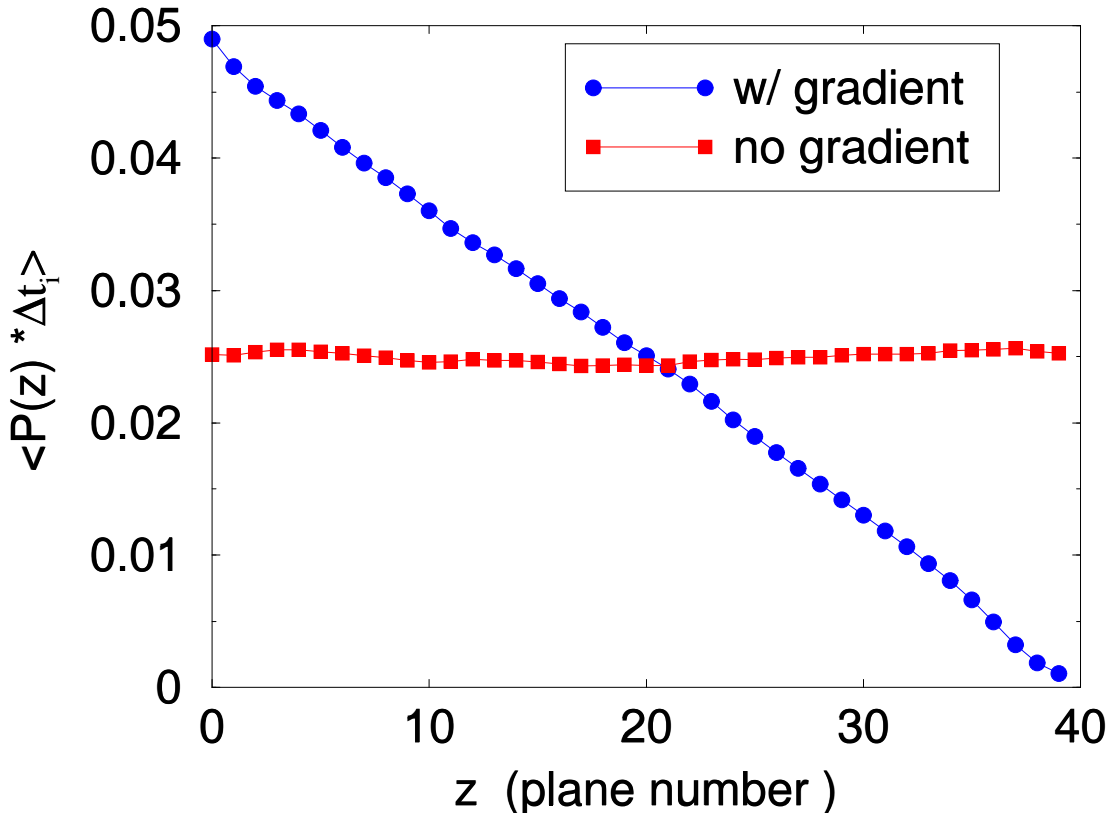
Figure 4.1: Time-averaged probability of finding a vacancy one of the (001) planes, perpendicular on the gradient direction (labeled from 0 to 39) from KLMC simulations with and without a vacancy gradient present. The number of sites was 8×10^3; the bias parameter b=2.

gradient direction (we have four equidistant planes per unit cell) has a constant gradient, while there is no dopant gradient.

From Eq. 4.4 we see that γ can be found if we know the dopant flux and the dopant diffusivity, with a vacancy gradient present as shown in Fig. 4.1. The dopant flux is calculated from the dopant mean displacement. As was observed in lattice-gas models for binary alloys[20], the mean displacement is self-averaging, hence we monitored this quantity for sufficiently long times. This technique allowed us to obtain more accurate results than in our earlier work[25]. In Fig. 4.2, one can see the mean displacement versus time for As at different temperatures. While the mean
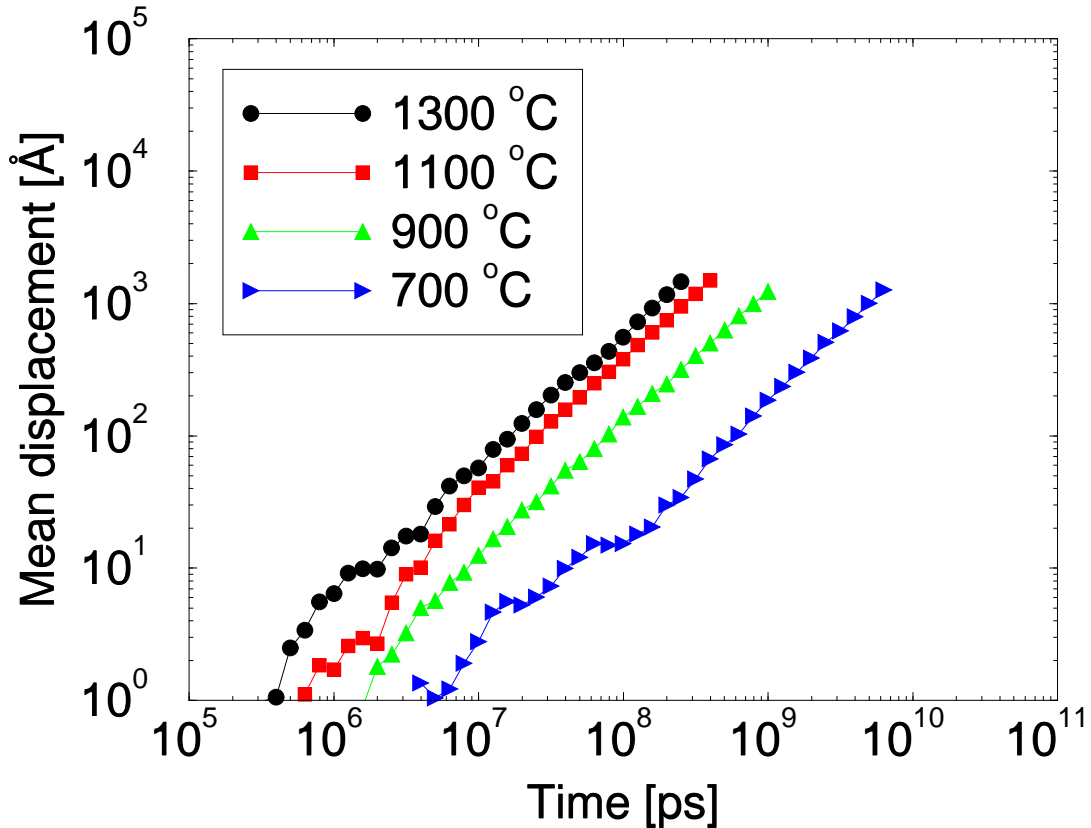
Figure 4.2: Mean displacement of As as function of time in a vacancy gradient for different temperatures. The number of sites was 8×10^3, the bias parameter b=2.

squared displacement of the dopant in a vacancy gradient could be used to find dopant diffusivity by subtracting the drift term, the diffusivity obtained in this way is noisy and a run with no vacancy gradient was preferred. Mean squared displacement for As at four temperatures is shown in Fig. 4.3.

Shorter times were used and many more simulations (a few hundreds) were performed to reduce statistical errors. Tests performed for As at 1300°C with cells of 6.4×10^4 sites found the same value for γ as with 8×10^3 sites, so the smaller system was used for the bulk of the simulations. For mean displacements larger than 50 Å, the standard deviation of the mean is smaller than the size of the symbols in Fig. 4.2 and as such it is not shown.
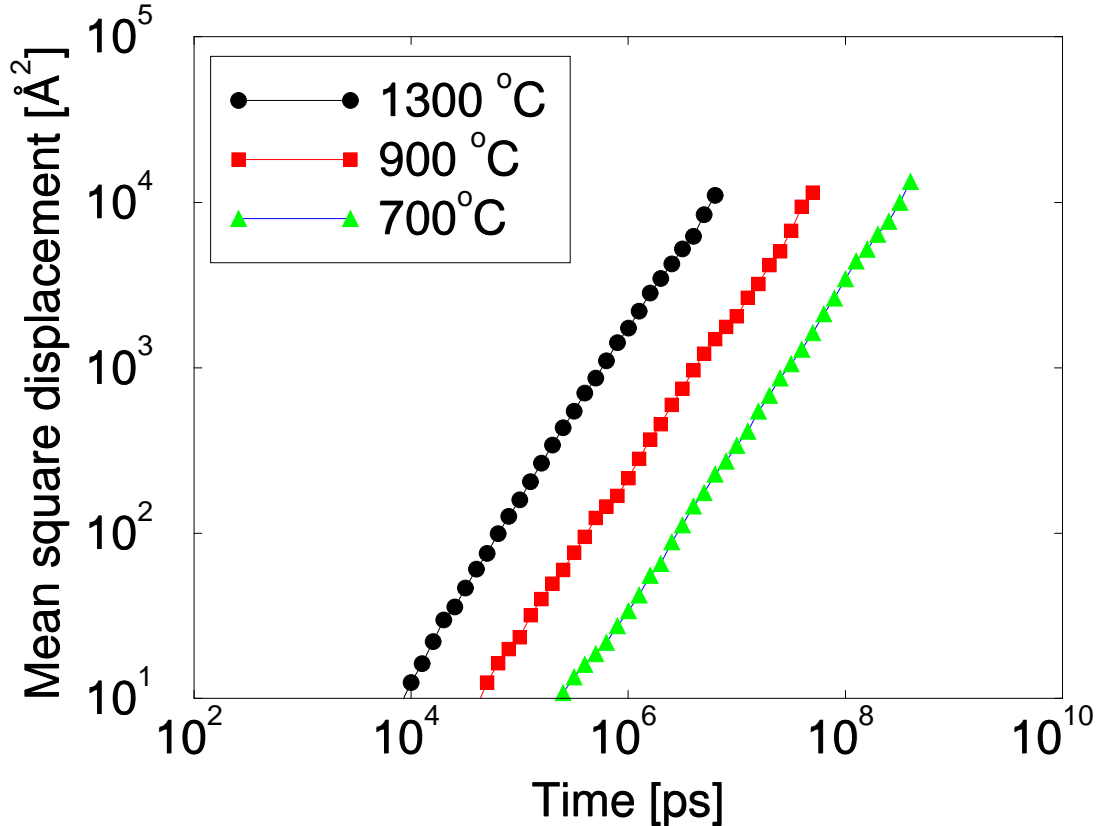
Figure 4.3: Mean squared displacement of As as function of time with no vacancy gradient for different temperatures. The number of sites was 8×10^3, the bias parameter b=2.

We can look first at the diffusivity versus temperature as a test of the KLMC simulations and our understanding of the diffusion processes. For vacancy-mediated diffusion, a vacancy must separate to third-nearest neighbor distance and return along a different path in order for long-range diffusion to occur. Thus, for As, the pair diffusivity depends on the activation barrier between nearest neighbor binding and the second to third neighbor transition For KLMC simulations with one vacancy and one dopant, the As-V pair diffusivity ($\propto \exp(-0.96/k_B T)$) must be corrected by the probability that the dopant and vacancy are paired $[1 + 2000\exp(-1.17/k_B T)]^{-1}$. This correction is more significant at high temperatures, leading to curvature on the
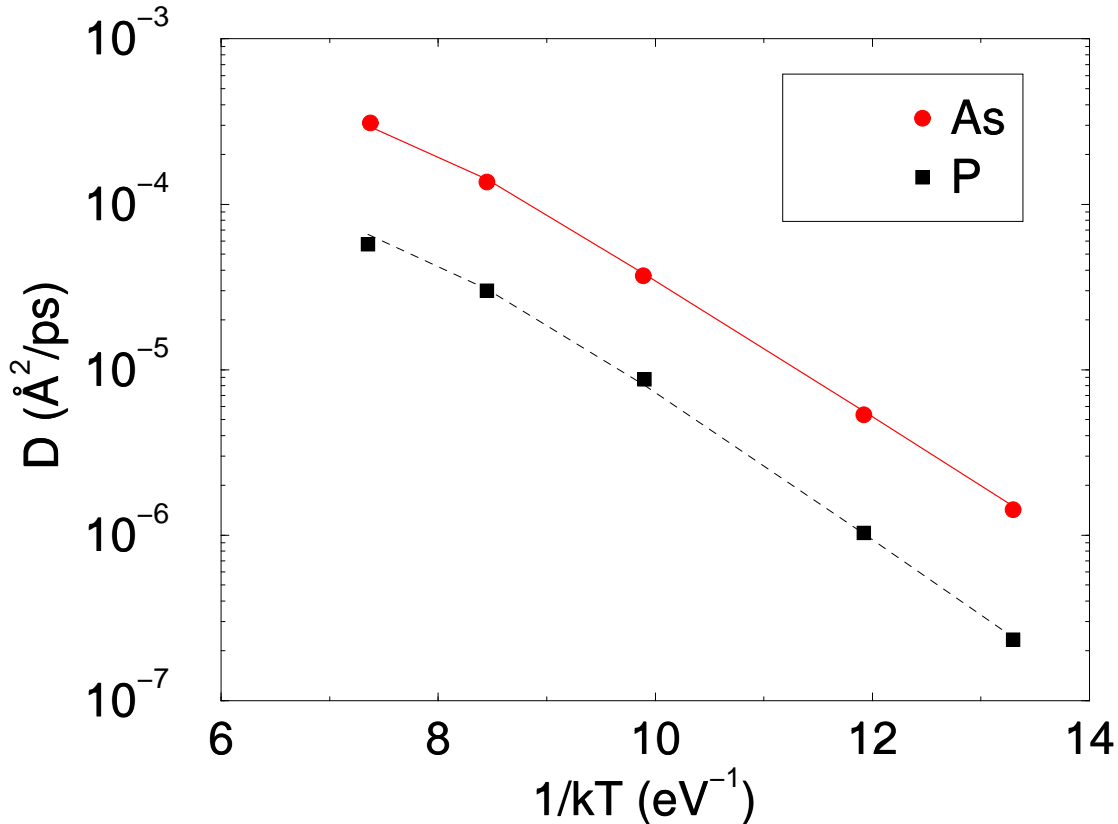
Figure 4.4: The As and P diffusion coefficients versus temperature from kinetic lattice Monte Carlo simulations with 8×10^3 sites, one dopant and one vacancy, and no vacancy gradient. As diffusivity ($\propto \exp(-0.96\mathrm{eV}/k_B T)$) and P diffusivity ($\propto \exp(-1.05\mathrm{eV}/k_B T)$) are corrected by the probability of a site, first nearest neighbor from the dopant, to be occupied by a vacancy, relative to the occupation probability of a site far away from the dopant, $(1 + 2000\exp(-1.17\mathrm{eV}/k_B T))^{-1}$, and $(1 + 2000\exp(-1.05\mathrm{eV}/k_B T))^{-1}$, respectively.

Arrhenius diffusivity plot (as seen in Fig. 4.4).

Since the number of vacancies is fixed the formation energy of a vacancy is not included. For P, pair diffusivity is limited by the large exchange barrier (1.05 eV), which is well above that for the second to third neighbor transition (0.72 eV). Note that the KLMC simulation does not include the vacancy formation energy.

For As in a vacancy gradient, we find (Fig. 4.5) that the correction factor γ is positive, meaning that the As flux is in the same direction as the vacancy flux. At
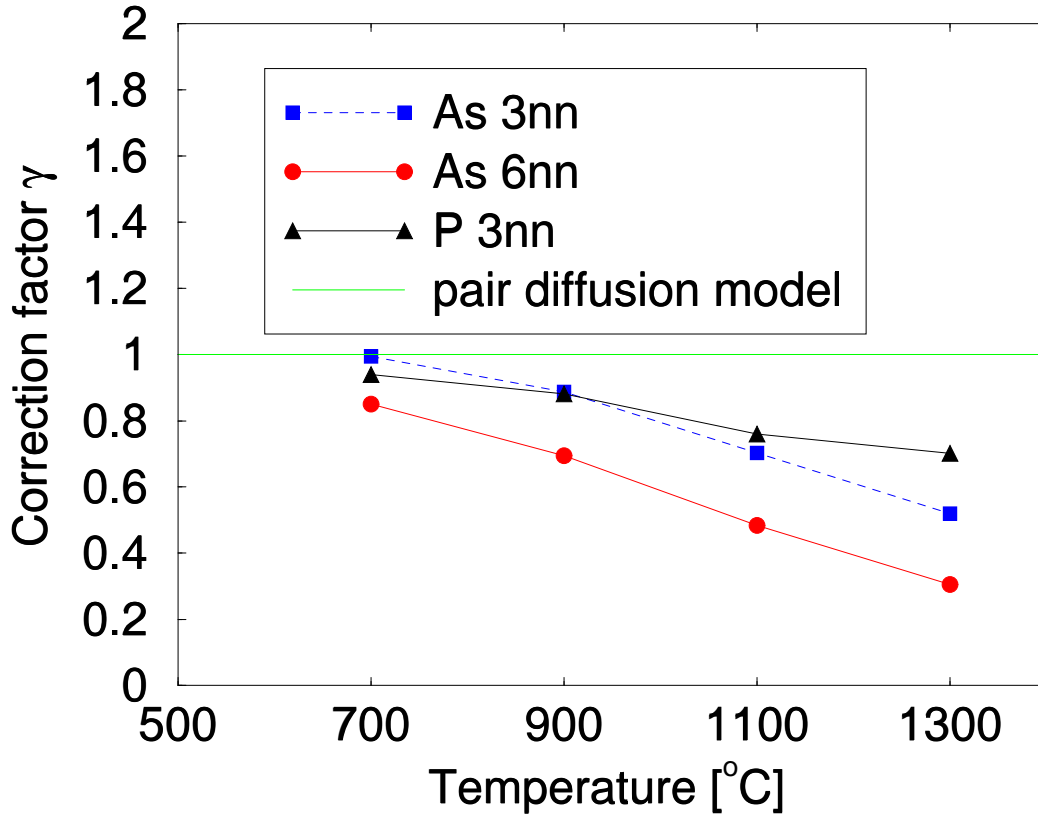
Figure 4.5: Correction factor γ from kinetic lattice Monte Carlo simulations for As and P as a function of temperature and range of interaction (3nn: third nearest neighbor, 6nn: sixth nearest neighbor. The number of sites was 8×10^3, the bias parameter b=2.

700°C, γ is close to one, matching the prediction of the pair diffusion model. At higher temperatures, however, γ drops, with a value at 1300°C of about one third the value predicted by the pair diffusion model.

The basis for this behavior can be understood by considering the microscopic processes. Pair diffusion assumes that the pair is strongly bound and makes many hops before dissociating. As the temperature rises, the thermal fluctuations k_BT become larger relative to the difference in activation energy between pair diffusion and dissociation, reducing the number of hops made before the pair breaks up. At the same time, the first dopant hop is likely to be in the direction *opposite* the vacancy

flux as that is the direction from which the V is more likely to approach. As the number of hops for a pair drops, the bias induced by the first hop becomes more important dropping γ, which depending on the interaction potential, can become negative[24], approaching the -2 value seen for tracer diffusion (in agreement with the statistical model of List *et al.*[15]).

The values of correction factor γ are smaller if interactions up to sixth nearest neighbor (current ab-initio results are available only up to this range for As) are taken into account. This can be understood by noting that a longer-range interaction is associated with a larger effective capture cross-section, and thus conversely also an increased dissociation rate.

For P, the large exchange barrier leads to two significant changes relative to As. First, the large barrier reduces the number of hops made by the pair before breaking up, thus tending to reduce γ. Second, since exchange is inhibited, captured vacancies are likely to diffuse in the neighborhood of the dopant (separating to third neighbor distance and returning) before exchanging, greatly reducing the bias associated with the initial hop. The net result of these two compensating effects is a weaker temperature effect than for As. At lower T, γ is smaller for P than for As, while at higher temperatures P has a larger value of γ than As (Fig. 4.5).

Recent *ab-initio* calculations were used to describe the attractive interaction between a dopant and a vacancy in KLMC simulations of dopant diffusion in a vacancy gradient. It is found that for As the dopant flux driven by a vacancy gradient has the same direction as the vacancy flux with a magnitude that approaches that of ideal pair diffusion at low temperatures (700°C) and drops with increasing temperature. The dopant flux decreases if long range interactions are taken into account. Due to a large exchange barrier which becomes the rate limiting step for pair diffusion, P has a similar behavior, but a weaker temperature dependence, leading to dopant fluxes

which are smaller at low T, but larger at high T.

4.2   Capture Radius for Frenkel Pair Recombination

Ion implantation is an efficient method for introducing dopants in silicon.[27] The implantation process produces considerable lattice damage due to the energetic collisions of ions with the lattice atoms.

In continuum models[17] as well as Monte Carlo simulations which do not replicate the silicon lattice,[31, 32] the annihilation between vacancies and interstitials is described by a capture radius which is not well characterized. Previous TBMD calculations[12] showed that there is a long range interstitial-vacancy interaction extending up to the sixth-nearest neighbor distance. In order to quantify the interstitial-vacancy interaction more completely, molecular dynamics calculations were performed using a recently developed environment dependent interatomic potential (EDIP).[33, 34, 35] Those results are then used in KLMC simulations to determine the capture radius for Frenkel pair recombination and how it depends on the interaction range.

Constant temperature MD with environment dependent interatomic potential (EDIP)[33, 34, 35] was used for the calculation of the interaction potential between interstitials and vacancies as a function of relative location. For each configuration, the atomic positions were relaxed at 0.1K to obtain the total energy of the system. Our calculations confirm that the $\langle 110 \rangle$ split interstitial is the lowest energy configuration for a single self-interstitial with formation energy of $E_I^f = 3.4\text{eV}$. The calculated vacancy formation energy is $E_V^f = 3.2\text{eV}$. A 512 atom supercell was used.

Test calculations with supercell size of 1728 atoms give formation energies within 0.1 eV.

Initial conditions in KLMC method are obtained a) by having the vacancy and the Si self-interstitial randomly located on a 3D lattice, as in the case of finding the capture radius for I-V recombination as function of interaction range. Transition rates for vacancy and interstitial satisfy detailed balance and are postulated to be as in Eq. 4.5:

$$\nu = \nu_m \exp\left(\frac{E_i - E_f}{2kT}\right), \tag{4.7}$$

where ν_m is the migration frequency, k is Boltzmann's constant, T is the absolute temperature, and $E_i - E_f$ is the change in the system energy associated with a possible hop. The values of ν_m associated with interstitial and vacancy hops are chosen so that the diffusivities of isolated point defects match the TBMD[12] values of $D_v = 1.18 \times 10^{-4}\exp(-0.1/kT)$ cm^2/sec and $D_i = 0.158\exp(-1.37/kT)$ cm^2/sec.

I-V interactions energies versus distance are calculated via MD calculations as described above. Vacancy-vacancy and interstitial-interstitial interactions are chosen to match cluster binding energies from Jaraiz et al.[31] Only hops to first nearest neighbor sites are considered.

Periodic boundary conditions are considered for I-V capture radius calculations. The MD simulation results for interstitial-vacancy interaction is presented first. ' As initial conditions, a split interstitial is placed at one site and an atom is removed from another site creating a vacancy. The system is then relaxed via MD and the energy and configuration saved. This process is repeated for different initial vacancy-interstitial displacements. We find that the vacancy-interstitial interaction potential depends strongly not only on distance, but also on direction (Fig. 4.7). Specifically,
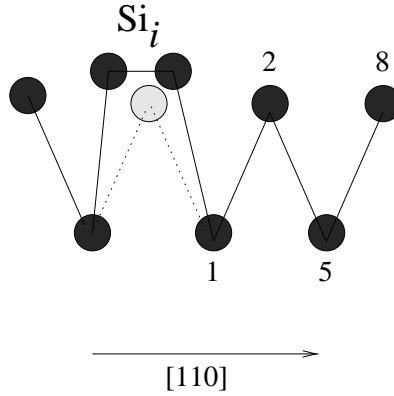
Figure 4.6: Numbers enumerate n-th nearest neighbor lattice sites for the vacancy relative to the split interstitial.

at short range the binding energy is much larger for vacancies located in the direction of buckling of the split interstitial ("up" in Fig. 4.7), with minimal binding even for close proximity in the opposite direction ("down"). The analysis shows that long range interactions are present, particularly along the $\langle 110 \rangle$ chain oriented in the direction of the split interstitial (0.6eV at fifth nearest neighbor distance).

In continuum[17] and off-lattice Monte Carlo[31, 32] models for dopant diffusion in silicon, the annihilation between a vacancy and a self-interstitial is described by a rate constant:

$$k_{I,V} = 4\pi a_{I,V}(D_I + D_V),$$
(4.8)

where the capture radius $a_{I,V}$ is often chosen arbitrarily. Since KLMC simulations explicitly include the silicon lattice structure, the Frenkel pair recombination rate $k_{I,V}$ and thus the capture radius can be calculated based on the I-V interaction potential as obtained from MD. Using initial random I and V displacements within
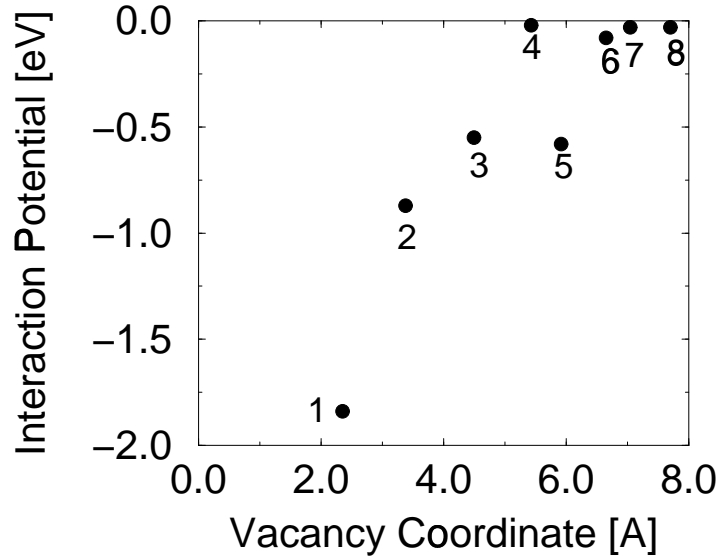
Figure 4.7: EDIP potential has been used to calculate the interaction potential between an interstitial and a vacancy as a function of distance. A long-range binding was found which depended strongly on the displacement direction relative to the orientation of the split interstitial. The distance (vacancy coordinate) is measured relative to the ideal lattice sites where interstitial and vacancy were introduced.

a simulation box of volume Ω, the recombination rate is given by:

$$k_{I,V} = \frac{1}{\langle\tau\rangle\Omega},\tag{4.9}$$

where $\langle\tau\rangle$ is the average recombination time. In Fig. 4.8, one can see that for short range interaction (first nearest neighbor binding which results in second nearest neighbor capture) the capture radius is $3.5\,\AA$. The capture radius is $6.7\,\AA$ if long range interaction is taken into account (up to sixth nearest neighbor). With no I-V interaction (and thus only nearest-neighbor capture) the capture radius is $2.21\,\AA$. These calculations were performed at $900°C$. It is found that the capture radius increases slightly as the temperature is reduced, as might be expected since at low
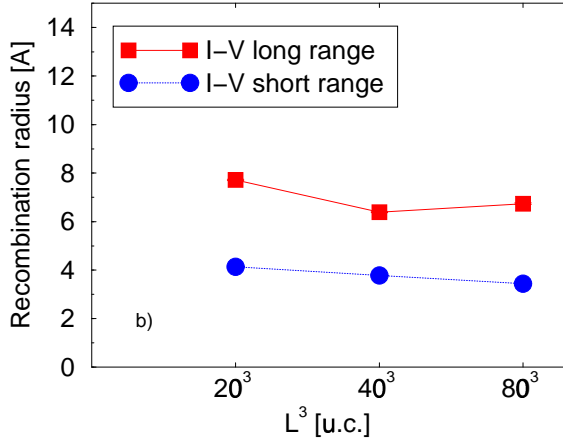
Figure 4.8: Capture radius for Frenkel pair recombination ($a_{I,V}$) with short (1NN) and long (6NN) range interstitial-vacancy binding as calculated with different system sizes expressed in number of unit cells.

T the capture probability increases for the weaker binding energies seen at larger distances.

Molecular dynamics calculations show the existence of a long range interaction between vacancies and silicon self-interstitials which extends up to eigth nearest neighbor. This interaction is dependent on separation distance, but also on the direction of displacement of the vacancy with respect to the orientation of the split interstitial. This long-range interaction increases the the rate of Frenkel pair recombination.

Chapter 5

Anomalous Diffusion in Highly Doped Silicon

5.1 No Fermi Level Correction

In diffusion of dopants at very high concentrations anomalous behavior has been observed. Rapid thermal annealing (RTA) experiments by Larsen[40] made at 1050°C for 10 seconds indicate that below a threshold concentration ($\sim 2 \times 10^{20}$ cm^{-3}), the diffusivity of group IV and V impurities (As, Sb, Sn and Ge) increases linearly with dopant concentration, while above this concentration the diffusivity increases dramatically with increasing donor concentration ($\propto$ C^n, n$\sim 3-6$). Earlier investigations [41] carried out over longer times (several hours) found that in the temperature range 1000–1100°C, the diffusivity of dopants (As) decreases rather than increases at very high concentration (see Fig. 5.1). Mathiot and Pfister proposed a percolation model while Dunham and Wu proposed a Lattoce Monte Carlo approach which provides a better description taking into account quantities like correlation factor, interaction range and random location of defects.

38
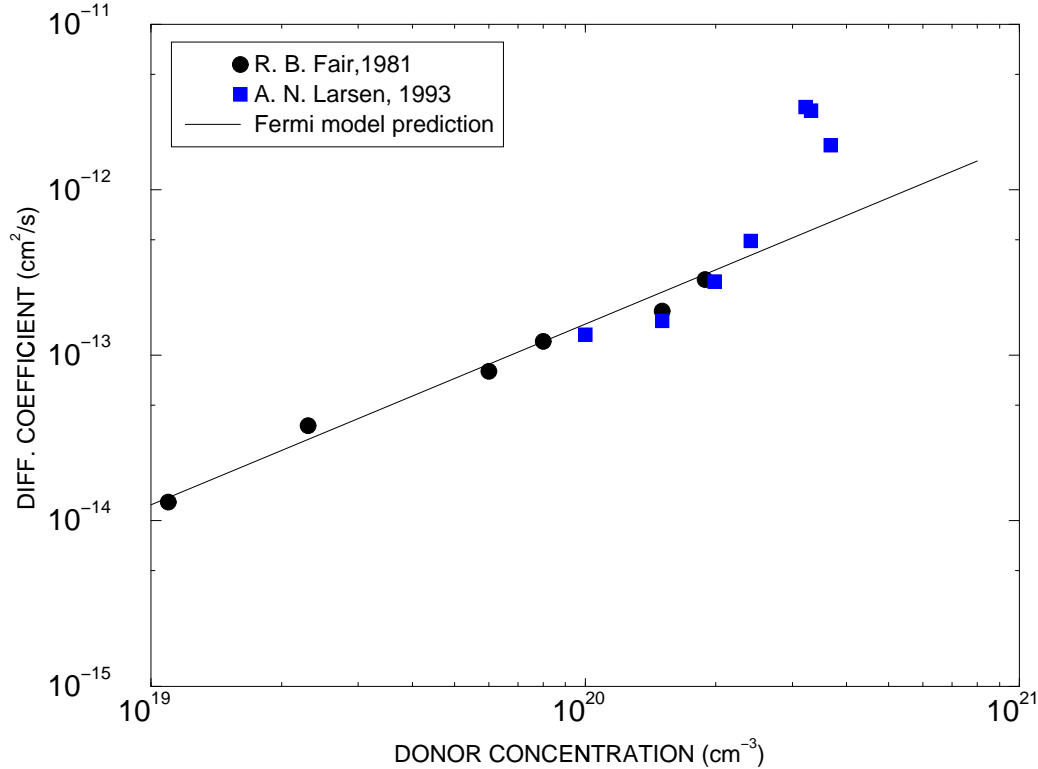
Figure 5.1: Diffusion coefficient as function of dopant cncentration from isoconcentration experiments by Larsen *et al.* and from Fair *et al.*

On the other hand impurity diffusion and aggregation depend on the underlying atomic-level processes. Recently it has become possible to use *ab-initio* calculations based on density functional theory (DFT) and the local density approximation (LDA) to investigate these atomic-scale processes. As an example that will be applied in this work, the binding energies for dopants, vacancies and related clusters in silicon have been calculated as functions of the local configuration by several groups [5, 7, 38] (see Chapter 2). In contrast with simple pair diffusion models which provide the basis for most continuum modeling, these calculations show that relatively long-range interactions exist between dopants and vacancies (out to at least tenth nearest neighbor distances). The presence of long-range interactions opens the door for relatively

complex interactions among multiple dopants with multiple vacancies, particularly at high doping levels.

In order to explore how the nature of these dopant-vacancy interactions controls macroscopic diffusion and aggregation behavior, the Kinetic Monte Carlo method is applied.

In the KLMC simulations, periodic boundary conditions are used on a three-dimensional (3D) array of cubic cells, each with 8 lattice sites as in the silicon (or diamond) structure. Dopant-vacancy interactions are specified in terms of energy as a function of atomic configuration. Interactions energies are assumed to be additive, an assumption which is close to what is found by *ab-initio* calculations[38]. To initialize the system, dopants are placed randomly within the 3D structure according to the designated doping density. The vacancies are then placed with the probability of occupation depending on the binding energy for each site as calculated based on the dopants in the neighboring region:

$$p_V = \frac{p_V^0}{p_V^0 + (1 - p_V^0)\exp(\Delta E/kT)} \tag{5.1}$$

where p_V^0 is the probability of occupation for sites far from any dopant atom, k is Boltzmann's constant and T is the absolute temperature. The energy ΔE is:

$$\Delta E = -\sum_{i=1}^{n} n_i \Delta E_i, \tag{5.2}$$

n_i being the number of dopants atoms as i^{th}-nearest neighbor and ΔE_i the corresponding dopant-vacancy binding energy. We consider values of n between 3 and 6 in this work, since as recognized by Hu[39], long range migration of a dopant via vacancy-mediated diffusion requires separation to the third-nearest neighbor (3NN)

site with respect to a dopant, while the long-range migration of an As_2V complex requires dopant-vacancy separation to a 6NN distance. Values for the arsenic-vacancy binding energies are used from the *ab-initio* calculations of Pankratov[5] see Table 1, Chapter2. The system evolves by considering the hopping of vacancies (actually the hopping of adjacent atoms onto the vacant site) with transition rates from Eq. (3.10). At each step, we update the hopping rates for vacancies, choose a hop based on the relative rates, and increment the time. In the end, the mean squared displacement is calculated to obtain the diffusivity.

Previous calculations [23, 24] using rough estimates of dopant-vacancy binding energies provided good agreement with the experimental observations of Larsen[40], predicting both the doping level at which the onset of enhanced diffusion occurs and as well as the dependence of diffusivity on increasing concentration. Using parameters from *ab-initio* calculations in the framework of 3NN interactions, again a strong enhancement in diffusivity for high doping levels and short simulation times is found (see Fig. 5.9, noting that Fermi level effects have been normalized out). However, at longer simulation times is found that the diffusivity enhancement decreases substantially (see Fig. 5.3), in agreement with experimental observations at longer times [41], the phenomenon being more pronounced at high doping levels. A comparison between diffusivity drop with time for different dopant concentrations is also shown in Fig. **??**. To understand this behavior the evolution in the number of As_xV complexes in the system is examined (see Figs. 4(a) and 4(b). The role of As_xV complexes in the overall diffusion process has been discussed recently by Ramamoorthy and Pantelides[38]. Based on their calculations, they proposed As_2V to be mobile and to have a significant role in the dopant diffusion. What KLMC simulations find is that because of the strong dopant-vacancy binding, at high doping levels the number of As_2V complexes is higher than the number of AsV pairs
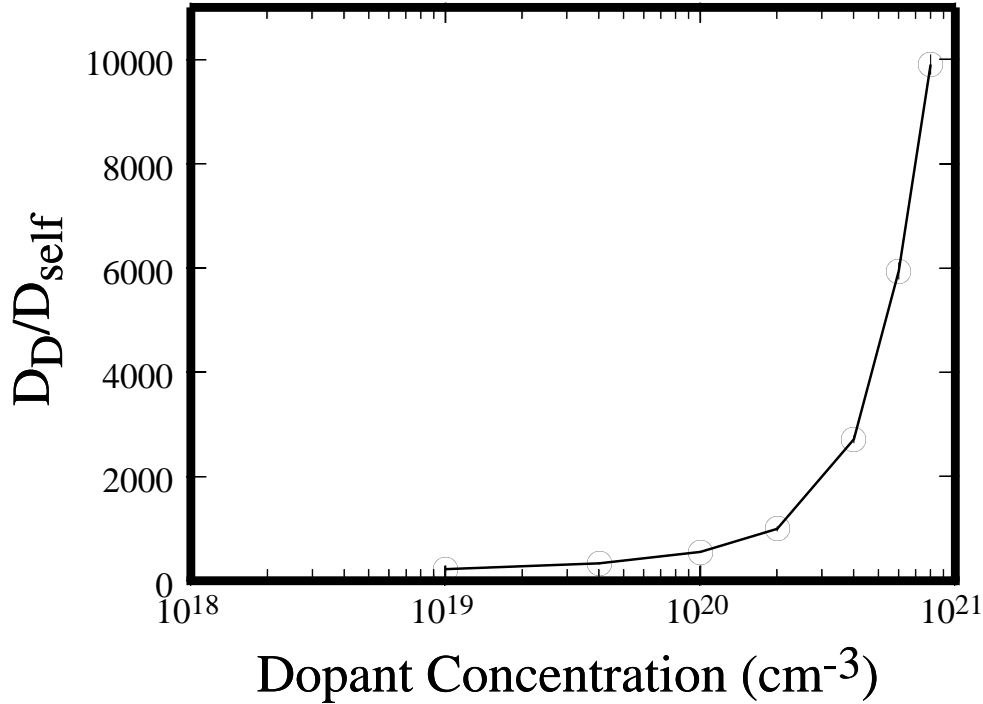
Figure 5.2: Normalized arsenic diffusivity versus doping density at 900°C from LMC simulations using *ab-initio* parameters[5, 6] after 10^4 t.u. 1 t.u. $= 1/\nu^0$ where ν^0 is the hopping frequency of a free vacancy. Note the strong increase above C$= 2 \times 10^{20}$cm^{-3}. The normalized diffusivity obtained by dividing by the vacancy component of silicon self-diffusion ($D_V C_V^*$), thus removing the Fermi level dependence.

and that their number grows with time, while the number of pairs decreases. As time progresses larger clusters such as As$_3$V and As$_4$V supplant the As$_2$V complexes. Since the larger complexes are much less mobile than the pairs, this is the source of the diffusivity reduction observed in our simulations.

To investigate further the role of As$_2$V complexes, the dopant-vacancy interactions is extended up to the sixth-nearest-neighbor (6NN) distance, since for long-range diffusion of the As$_2$V it is necessary for the vacancy to move away until it is at distances of 3NN and 6NN from the two dopants, respectively. By examining the
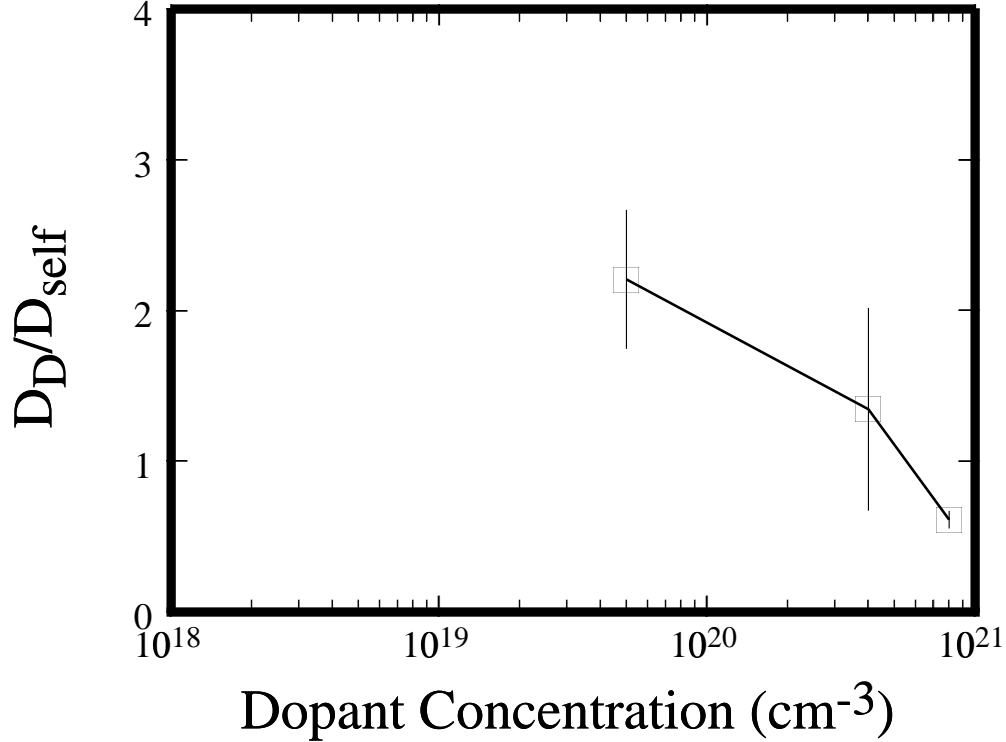
Figure 5.3: Normalized arsenic diffusivity versus doping density at 900°C from KLMC simulations using *ab-initio* parameters[5, 6] after 10^9 t.u. . The diffusivity actually drops rather than increases as in Fig. 5.9 due to clustering.

motion of isolated complexes (e.g., a one vacancy, two arsenic atom system), it is found that the diffusivity of As_2V complexes is about 50 times smaller than that of pairs at 900°C. However, as seen in Figs. 5.5 and 5.6, at high doping level the number of As_2V complexes greatly exceeds that of pairs, so these complexes can have a significant role in diffusion. In fact by combining the equilibrium concentrations of complexes with their diffusivity, it is found that for a concentration of 10^{20}cm^{-3} at 900°C, the contribution of As_2V to diffusion exceeds that of pairs (Fig. 5). However, a transition from diffusion dominated by pairs to domination by As_2V
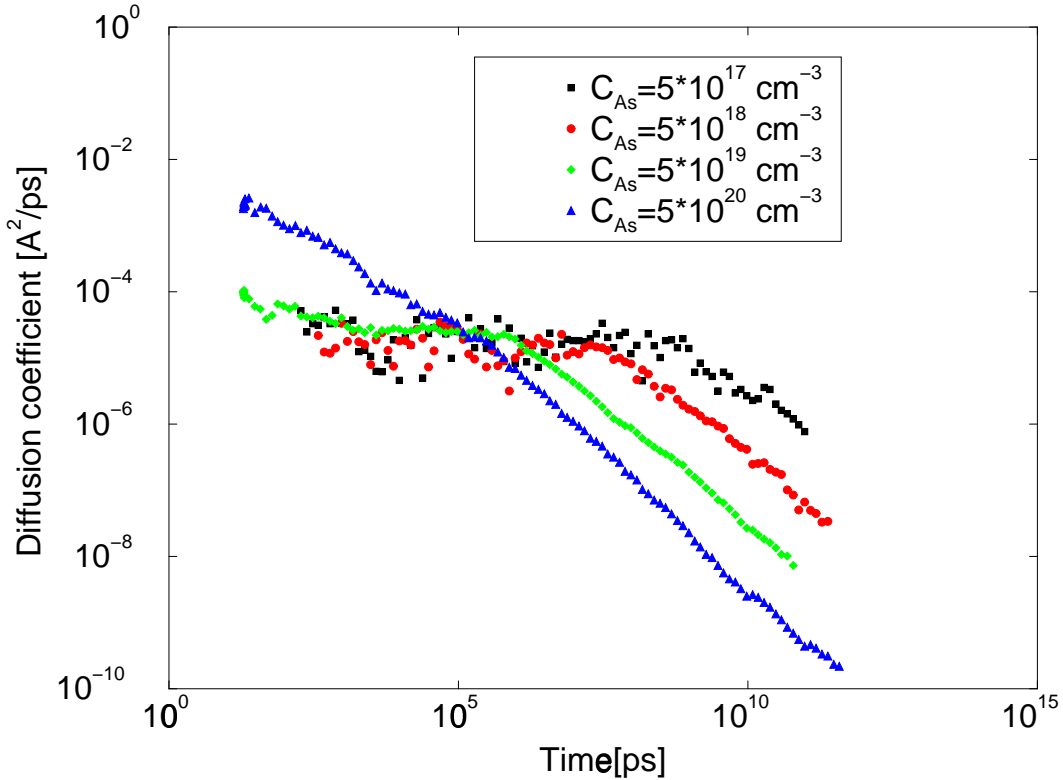
Figure 5.4: Arsenic diffusivity versus doping density at 900°C from KLMC simulations as function of time.

leads only to an increase of one in the order of the diffusivity increase with doping, in contrast to the much more abrupt increase observed both experimentally and in LMC simulations. Thus, although mobile complexes may play a significant role at high concentrations, the rapid increase in diffusivity with doping at very high levels is due predominantly to collective effects involving the interactions of vacancies with multiple nearby dopant atoms. Dopant/vacancy binding energies versus distance from *ab-initio* calculations [5, 7, 38] in lattice Monte Carlo simulations of vacancy-mediated diffusion in silicon. As observed experimentally [40], a strong diffusivity enhancement for arsenic in heavily doped silicon is found. Arsenic clustering takes place for longer times, again in agreement with experiments [41]. The role of mobile As_2V complexes was also explored, leading to the conclusion that these complexes
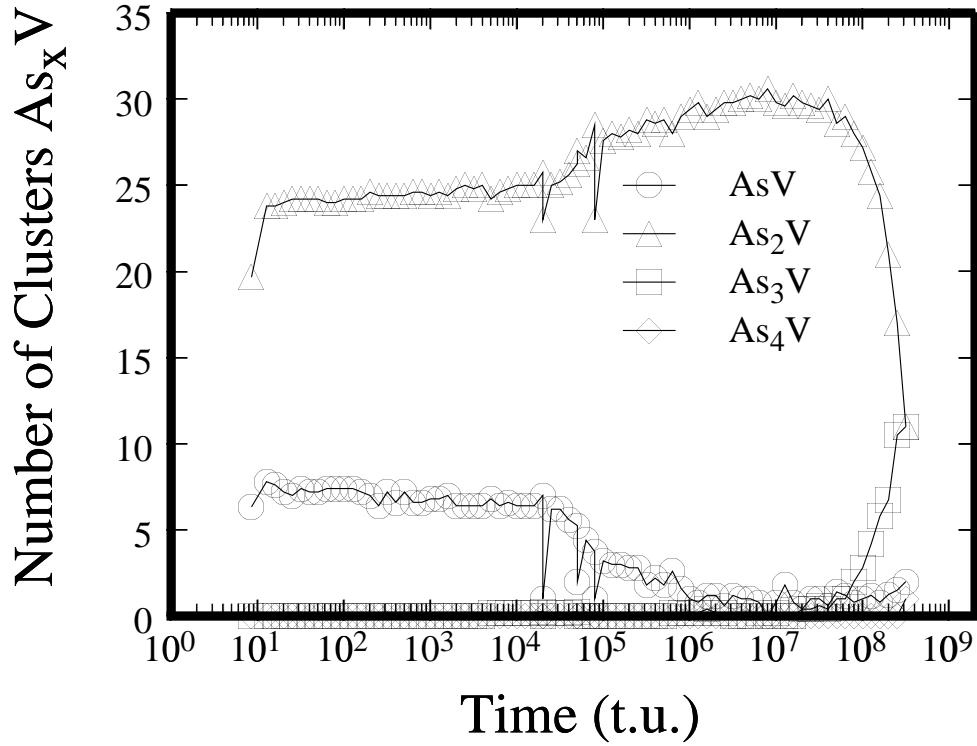
Figure 5.5: Number of $As_x V$ clusters versus simulation time at 900°C for dopant density of $5 \times 10^{19} \mathrm{cm}^{-3}$

are in fact mobile and can contribute significantly to diffusion, although their diffusivity is much smaller than the diffusivity of pairs, since they are present in higher numbers at high doping levels. However, the large enhancement in diffusivity at high doping levels is due primarily to collective effects involving the interactions of vacancies (even those in complexes) with several dopant atoms.
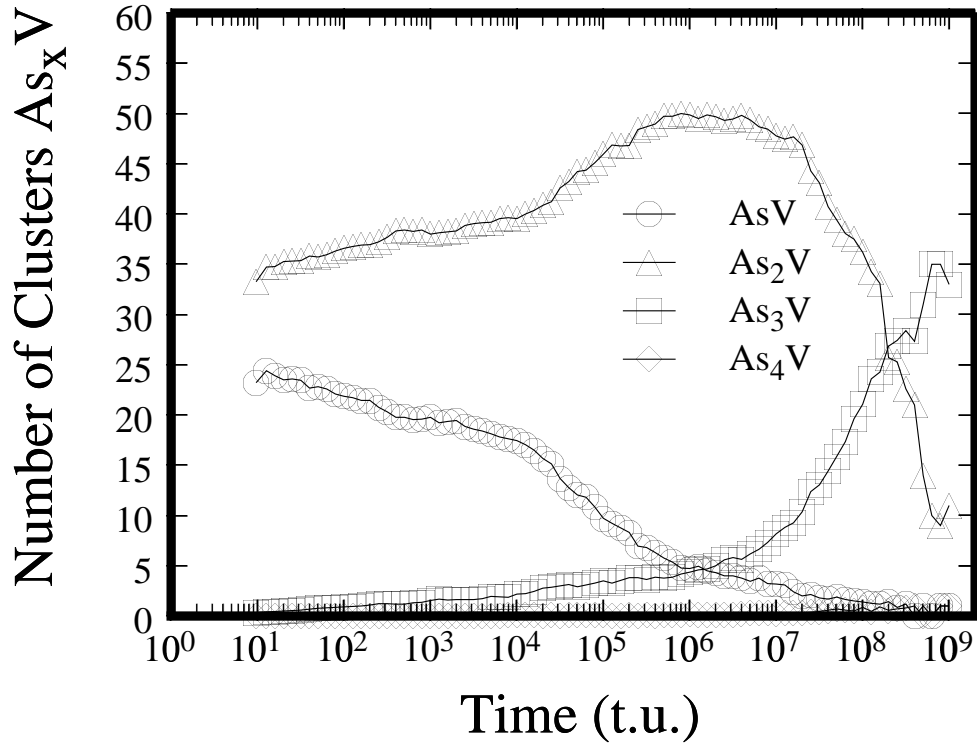
Figure 5.6: Number of As$_x$V clusters versus simulation time at 900°C for dopant density of 4×10^{20}cm^{-3}.

5.2 With Fermi Level Correction

As the doping level in silicon changes the position of the Fermi level changes also:

$$\frac{n}{n_i} = \exp(\frac{E_f - E_i}{kT}) \qquad (5.3)$$

As result if vacancies are assumed to single negatively charged then the concentration of vacancies is :

$$\frac{C_V^-}{C_V} = \exp(\frac{E_f - E_i}{kT}) \qquad (5.4)$$
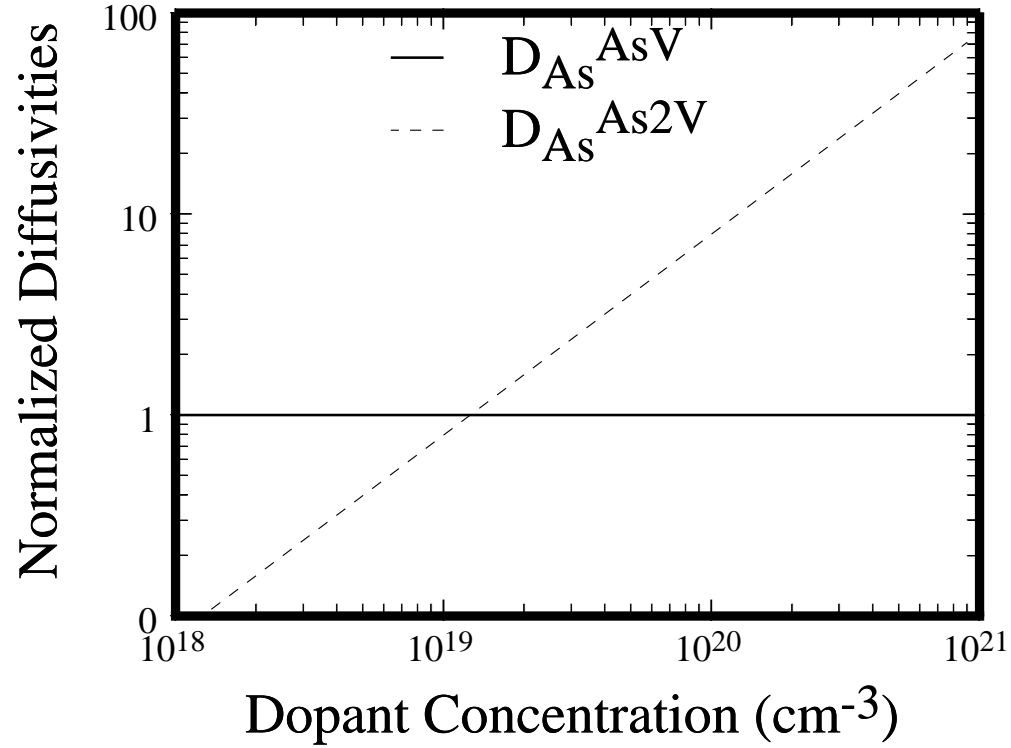
Figure 5.7: Relative diffusivities of arsenic due to AsV pairs and As$_2$V complexes versus doping level at 900°C. The contribution of As$_2$V to diffusion is predicted to dominate above C$_{As}$ = 2 × 10^{19}cm^{-3}.

One can see in Fig. 5.8 the mean square displacement for three different dopant concentration at 1050°C and $H_V^f = 3.65eV$, $S_V^f = 9k_B$, simulation box of 100^3 unit cells.
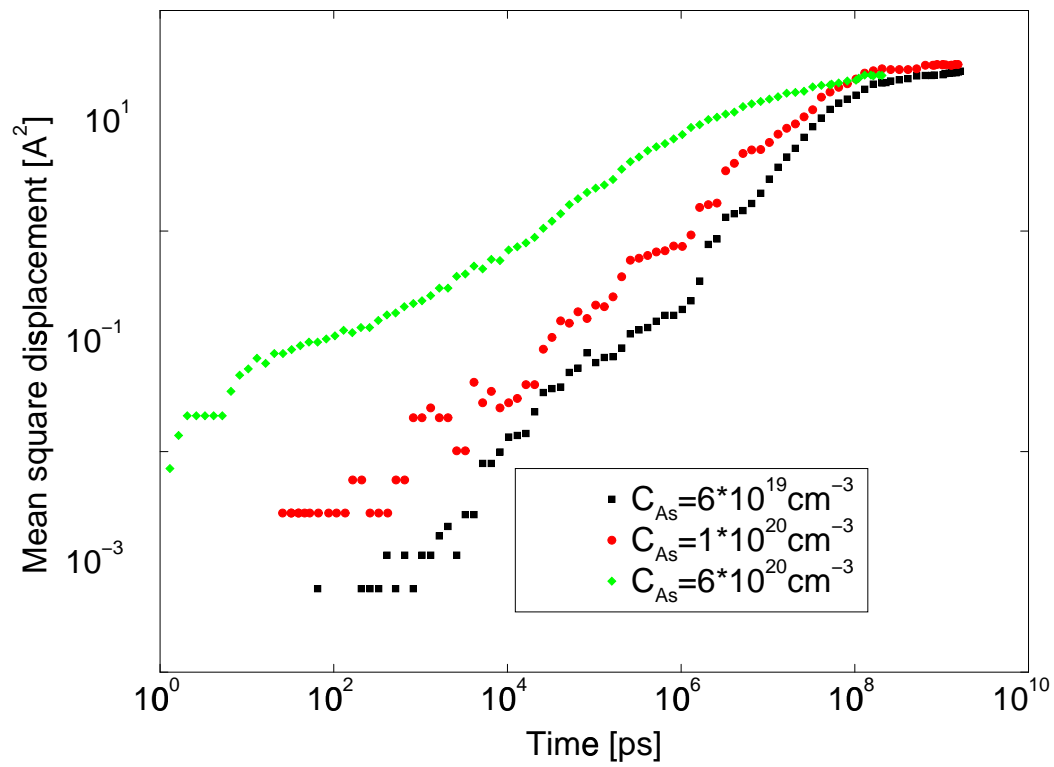
Figure 5.8: The mean square displacement os function of time for three different dopant concentrations at 1050°C including Fermi level effects
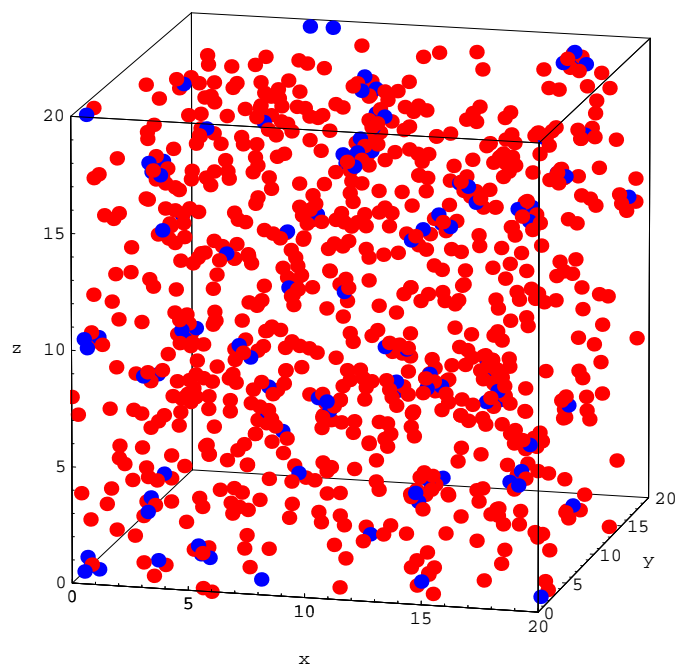
Figure 5.9: A 3D picture of dopants (grey atoms) and vacancies (black atoms) after a long simulation time when vacancies formed clusters with dopant atoms.

Chapter 6

3D Atomistic Simulations of Submicron Device Fabrication

It is predicted that by 2012[42] MOS devices will have 50nm channel lengths and 20nm junction depths. A device with these dimensions and a dopant concentration of 10^{19}cm^{-3} has only 500 dopants in the channel region with the number of clusters and precipitates even smaller. Therefore for deep submicron devices, the atomic scale behavior will be important. Kinetic Lattice Monte Carlo[23, 25](KLMC) has emerged as an effective method for evolving a 3D system to times accessible by experiments. There are two reasons for this. On one hand, the fundamental time step in KLMC is related to hops (the time between $10^{-9} - 10^{-6}$ s) rather than the vibration period ($10^{-14} - 10^{-13}$ s) as in molecular dynamics simulations. On the other hand, the method considers only dopants and defects present in the system ($10^{10} - 10^{21}$cm^{-3}), which is much smaller than the atom density (5×10^{22}cm^{-3}). As far as the comparison with continuum models goes, as the devices become smaller continuum models become more complex, while KLMC computational requirements scale with L^3 and are inherently 3D.

6.1   Ion Implant Simulation

A Monte Carlo ion implant simulation (UT-Marlowe[36]) is performed to generate a 3D distribution of dopants, interstitials and vacancies. The arsenic implant is a room-temperature implant, 5 keV, $4 \times 10^{14} \text{cm}^{-2}$ into (001) Si, 7° tilt, 30° rotation. Boron implant is also a room-temperature implant 5keV, 10^{14}cm^{-2} into (001) Si, 7° tilt, 30° rotation.

6.2   KLMC simulation

Following the ion implantation it is assumed that in the regions where the concentration of interstitials is higher than $5 \times 10^{21} \text{cm}^{-3}$ the material recristalizes and as result interstitials and vacancies are removed from these regions. Also, since the anneal that is to be simulated is done at 900°C and KLMC calculations show a fast interstitial vaacncy recombination at this temperature, nearest neighbor recombination for interstitials and vacancies is taken into account. The dopants and point defects are mapped to the nearest site on the silicon lattice. Then a box $75 \times 75 \times 200$ unit cells, which represents a quadrant of an NMOS transistor is chosen to be simulated using KLMC, the top surface, through which the implant has been made, is assumed to be a perfect sink for defects and all the other surfaces have reflecting boundary conditions. The mobile species considered in KLMC are vacancies, interstitials and dopant interstitials. Migration and binding energies used in simulations are presented in Table 1. For interstitial arsenic *ab-initio* results are not available, so arsenic interstitial interaction similar to boron is assumed but with smaller binding energy for the As_s-I pair and no binding for the As_i-As_s pair. In KLMC the transitions rates are calculated according to Eq. (3.10)

The 3D picture of the 50nm NMOS quadrant with the locations of dopants is presented in Fig. 6.1, shown immediately after the ion implantation, (time=0), and after the KLMC simulated annealing at 900°C for time=10ms and time=0.1s.

In Fig. 6.2 it is shown the total number of point defects and interstitial dopants as functions of time. Between 1 ps and $1\mu s$ vacancies and interstitials are present in large numbers, the dominant processes being vacancy-silicon exchanges, interstitial hops and interstitial vacancy recombination. Dopants go from interstitial to substitutional state, either due to dissociation or interaction with vacancies. Looking at the number of boron clusters in Fig. 6.3 one can see that mostly isolated boron interstitial is present.

Next during this period a time interval (1 to $100\mu s$) is found where most of the dopants are in substitutional state. After 10^6 ns vacancies exist mostly in the form of vacancy-arsenic clusters. It is shown in Fig. 6.4 a boron implant identical with the one used for initializing the MOS device. Here it is seen that vacancies disappear much faster. From 10^6ns one can also see that the boron starts being kicked out in interstitials. Initially one starts with isolated boron interstitials but, as boron interstitials migrates through the lattice pairs with boron substitutional and forms pairs. The number of pairs reaches a maximum at 10^8ns when there is also a peak in the total number of boron interstitials in Fig. 6.2.

Table 6.1: Simulation parameters. Binding energies up to first nearest neighbor only.

binding energies	migration energies	exchange, kick-in and kick out barriers
$E(As\text{-}V)$=1.18 eV[5]	E_m^V=0.3 eV[44]	$E_{exch}(As\text{-}V)$=0.66 eV[5]
$E(As_s\text{-}I)$=0.6 eV	E_m^I=0.9 eV[43]	$E_{exch}(B\text{-}V)$=2.5 eV[6]
$E(As_i\text{-}As_s)$=0.0 eV	E_m^{Bi}=0.3 eV[43]	$E_{kick-out}(B)$=1.0 eV[43]
$E(B\text{-}V)$=0.17 eV[6]	$E_m^{As_i}$=0.3 eV	$E_{kick-in}(B)$=0.6 eV[43]
$E(B_s\text{-}I)$=1.0 eV[43]		
$E(B_i\text{-}B_s)$=1.8 eV[43]		
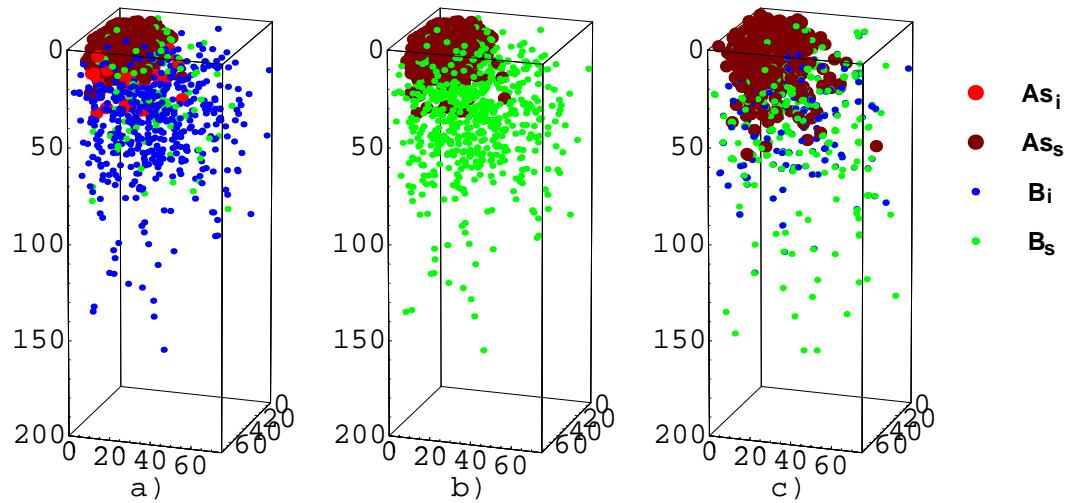
Figure 6.1: A quadrant (75×75×200 unit cells) of a 50nm nMOS transistor where dopants, arsenic and boron, in substitutional or interstitial state are shown, after ion implant simulation time=0 a). Also shown is the evolution of this system during an anneal at $900°$C at time=10^4ns b) and time=10^8ns c).
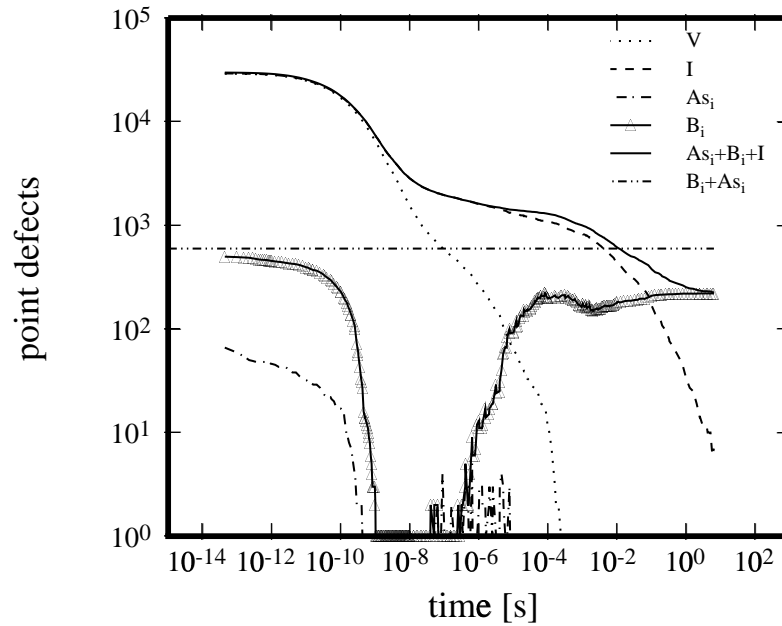
Figure 6.2: The number of vacancies, interstitials, dopant interstitials as function of time. The horizontal line represents the total number of dopant interstitials at the beginning of the KLMC simulation.

As the interstitials reach the surface where they are annihilated, there is not enough interstitials in the system for the number of pairs to keep growing. So they find more stable configurations in the form of bigger clusters: B3I (a boron interstitial with two substitutional boron as first nearest neighbor(1NN)), B4I (one B_i and three Bs as 1NN) and B5I one B_i and four Bs as 1NN). Given the energetics that is used here, these last clusters do not dissociate over the time that is simulated. It is expected that the big boron clusters grow and that small ones disappear freeing some interstitials in the process the same way the boron interstitial boron substitutional pairs decrease in favor of bigger clusters. It is found that the behavior of boron clusters is very much dependent on the binding energy of the boron interstitial boron substitutional pair. A simulation with only 1 eV for this energy produces much
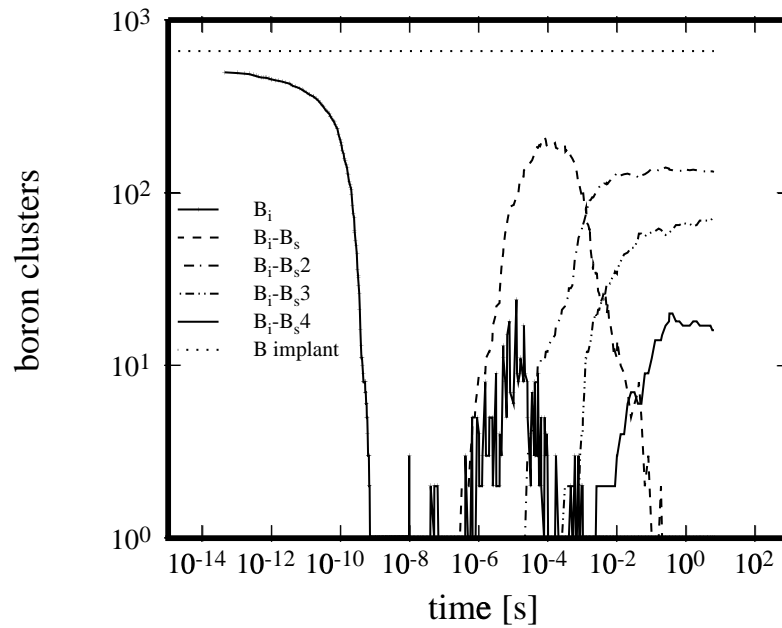
Figure 6.3: The number of boron interstitial clusters as function of time. Horizontal line is the number of boron atoms implanted.

less boron clusters. After 10s one can see that the number of total interstitials gets smaller than the initial number of interstitial dopants due to the perfect sink condition assumed for the top surface.

A time interval in which dopants are mostly substitutional is found. The presence of arsenic makes vacancies last longer in the system due to arsenic vacancy clusters. Simulating a 50nm MOs transistor is possible and further work will have to produce faster algorithms, since present simulations take about 50 hours as serial jobs on Origin2000. The dependence of energy on clusters size, and its influence on the overall system needs also further investigation, since the behavior of these clusters is very sensitive to the energies involved.
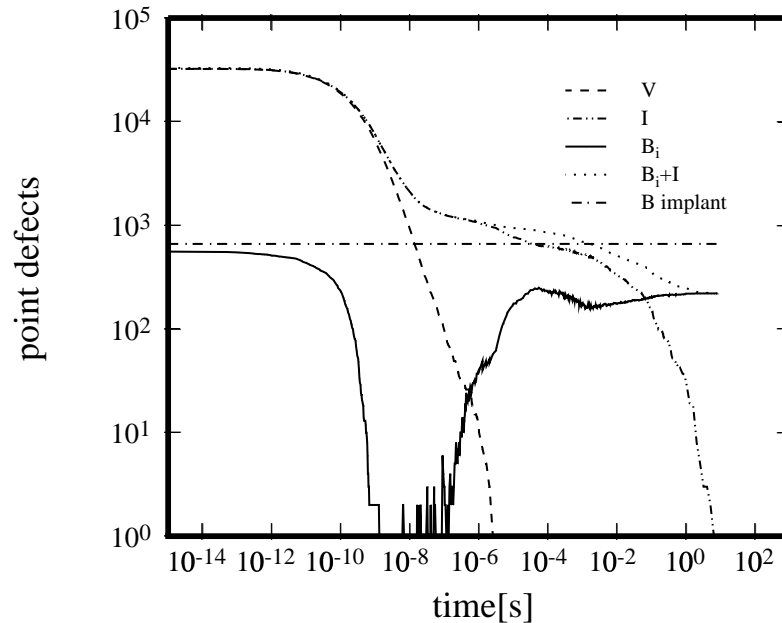
Figure 6.4: Number of vacancies, interstitials and boron interstitials as function of time for the annealing of a boron implant, 5keV, 10^{14}cm^{-2}, 7° tilt, 30° rotation. Horizontal line is the number of boron ions implanted.

6.3 The Si self interstitial excess as function of energy and dose

Ion implantation is an efficient method for introducing dopants in silicon.[27] The implantation process produces considerable lattice damage due to the energetic collisions of ions with the lattice atoms. Understanding the damage evolution following ion implantation is crucial for accurately modeling transient enhanced diffusion (TED).[28, 29] Present theories assume that TED is associated with the excess interstitials resulting from the implant damage, which aggregates into extended defects during annealing. The annealing process is often described through a +1 model[30] which assumes that after all Frenkel pairs generated during ion implantation recom-

bine, the number of interstitials left equals the number of implanted ions.

Corrections to the +1 model in the form of "effective +N" models[32] have been proposed to account for differences in TED associated with changes in implant species and ion energies. It was found that heavy ions leave a larger number of interstitials after Frenkel pair recombination due to the greater separation between interstitial and vacancy profiles. Here the initial stages of damage anneal are studied by using the interstitial-vacancy interaction described in Chapter 2.

Initial conditions in KLMC method are obtained a) by performing Monte Carlo implant simulations (UT-Marlowe[36]) that generate 3D distributions of dopants, vacancies and Si self-interstitials[37] (initial correlations) or b) depth distribution of point defects is like in a) but they are randomly located in the plane perpendicular on depth (no initial correlations). The implant ion is substituted by a Si self-interstitial. Transition rates for vacancies and interstitials satisfy detailed balance and are described by Eq. (3.10). The values of ν_m associated with interstitial and vacancy hops are chosen so that the diffusivities of isolated point defects match the TBMD[12] values of $D_v = 1.18 \times 10^{-4}\exp(-0.1/kT)$ cm^2/sec and $D_i = 0.158\exp(-1.37/kT)$ cm^2/sec.

Pair interactions are considered in determining system energies. The binding energy for vacancy-vacancy and interstitial-interstitial interactions as well as for vacancy-interstitial interactions are described by the following expression:

$$E_X(i) = \sum_{Y,j} E_{XY}[N_Y(j)], \tag{6.1}$$

where $E_X(i)$ is the sum of binding energies for a point defect X (vacancy or interstitial) at site i with other point defects Y within the range of interaction. For example, $N_I(1)$ is the number of interstitials as first nearest neighbor to a given site

and $E_{VI}(1)$ is the associated binding energy. I-V interactions energies versus distance are calculated via MD calculations[48] Vacancy-vacancy and interstitial-interstitial interactions are chosen to match cluster binding energies from Jaraiz *et al.*[31] Only hops to first nearest neighbor sites are considered.

The top surface is assumed to be a perfect sink and all the other surfaces are assumed to have reflection boundary conditions based on symmetry considerations.

The influence that the initial correlation of implant damage and the interstitial-vacancy interaction range has on the annealing behavior is studied through calculating the evolution in the net number of interstitials remaining (number of interstitials minus number of vacancies) as the Frenkel pairs generated during ion implantation recombine and diffuse to the surface. These excess interstitials are responsible for TED, which increases as the net interstitial excess increases. We define the +N number by the ratio of net interstitials to the implanted ions, which equals the interstitial excess in the +1 model. As shown in Fig.6.5 and Fig. 6.6, the value of N increases during recombination as the faster diffusing species (vacancies) diffuse to the surface. The +N factor after all the vacancies are gone is significantly reduced by both the initial correlation as well as the long range interaction. This is to be expected as both of these factors enhance the probability that a vacancy will recombine before diffusing to the surface.

Fig. 6.7 and Fig. 6.8 show how the +N factor depends on dose, implant energy, and modeling assumptions. The +N factor increases for lower doses, since the sparser damage increases the probability of vacancies making it to the surface. This increase is reduced when the initial defect correlations and long-range I-V interactions are included. The dependence on energy is more complicated. Although the effect is relatively weak, the +N factor appears to increase and then decrease with energy when the initial correlation is included, but only decrease with energy when the correla-
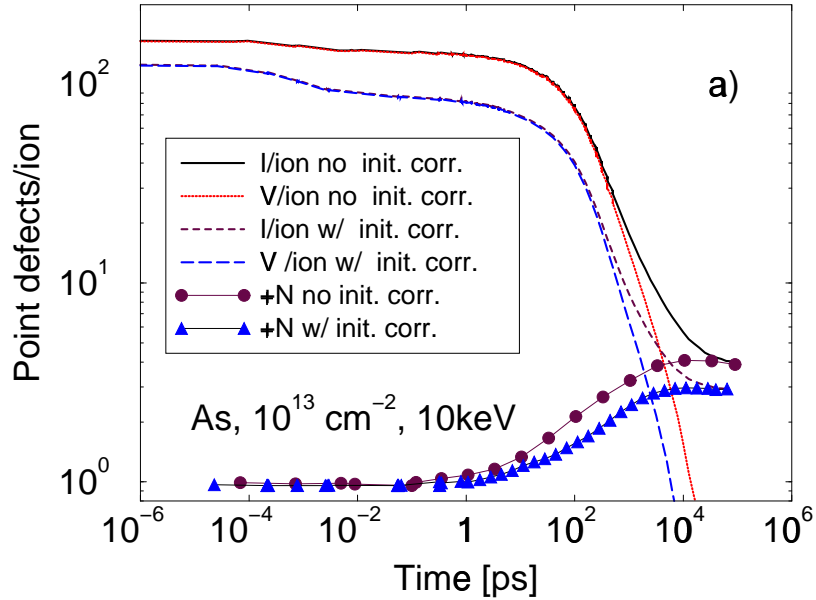
Figure 6.5: The number of point defects (vacancies and interstitials) per implanted ion and the +N number (net excess interstitials per implanted ion) as functions of time with and without initial correlations present for an As implant, 10 keV, 7° tilt, 30° rotation at 10^{13}cm^{-2} dose.
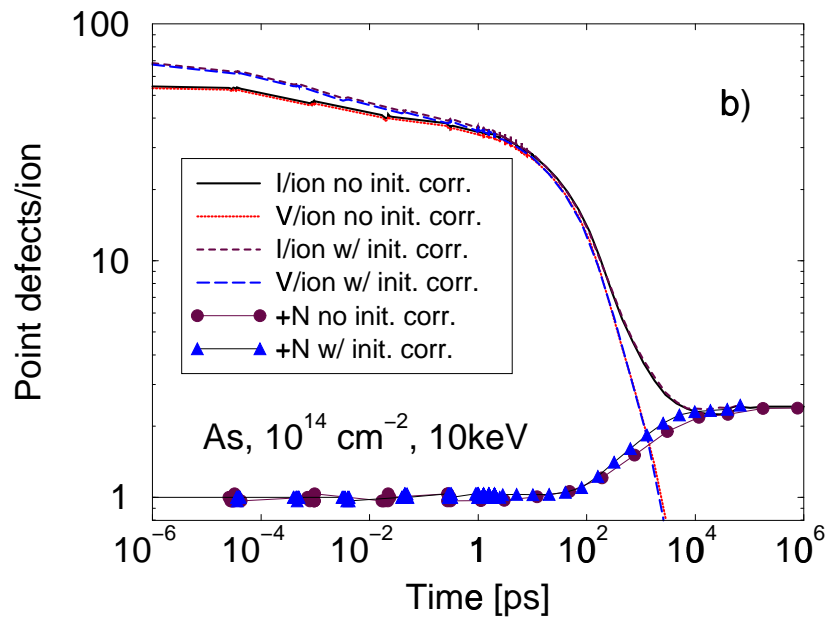
Figure 6.6: The number of point defects (vacancies and interstitials) per implanted ion and the +N number (net excess interstitials per implanted ion) as functions of time with and without initial correlations present for an As implant, 10 keV, 7° tilt, 30° rotation at 10^{14}cm^{-2} dose.

tion is ignored. A possible explanation for this behavior is that N decreases at larger energies because the damage is located further from the surface and thus vacancies are less likely to make it to the surface before recombining. At lower energies, the separation between I and V increases with energy due to the increased momentum transfer. This effect, which is only included when the initial defect correlations are included, reduces the initial probability of Frenkel pair recombination. This effect becomes less significant at higher energies as electronic stopping becomes dominant. For higher doses, the +N number appears to be almost independent of energy and modeling assumptions. This is due to the dense implant damage ensuring nearly complete Frenkel pair recombination. It may be noted that N does not reduce to 1, but instead to about 2 for arsenic implants. This is due to the separation between interstitial and vacancy distributions due to momentum transfer. When local Frenkel pair recombination is complete, a vacancy-rich region is left near the surface. These vacancies can diffuse readily to the surface, leaving greater than +1 excess interstitials.

Atomistic techniques were used to explore the initial phases of ion implant annealing in order to predict the resulting effect on transient enhanced diffusion. Kinetic lattice Monte Carlo simulations were used to calculate corrrections to the +1 model for effective damage distributions used in TED simulations as a function of dose, energy, and modeling assumptions. An effective "+N" factor was calculated which is proportional to the number of interstitials remaining after vacancies have recombined. This factor increases at lower doses since faster-diffusing vacancies can diffuse to the surface rather than recombining with interstitials. Using 3D damage distributions from MC implant simulations, it was found that the spatial correlations between vacancies and interstitials immediately following implantation is an important factor in determining the number of interstitials remaining after recombination. The long
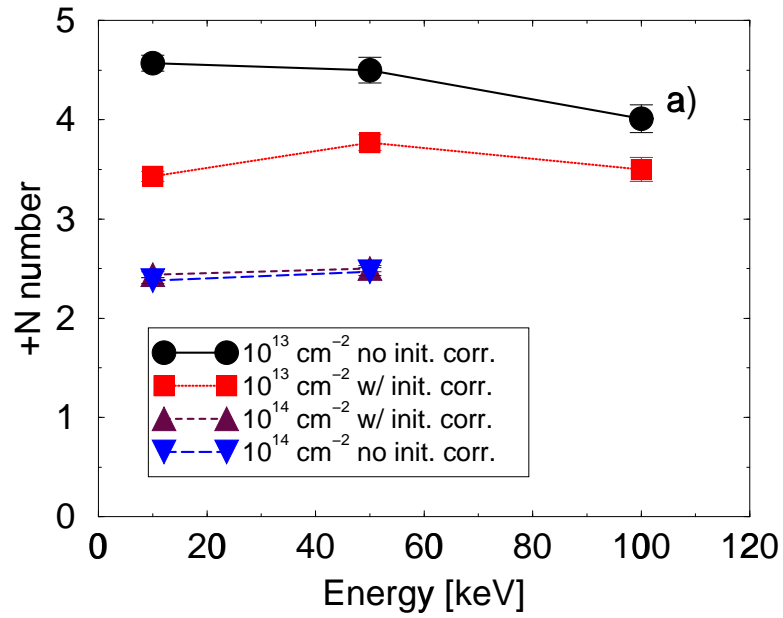
Figure 6.7: +N numbers after vacancies recombine for different doses and energies taking into account short range interaction between an interstitial and a vacancy. Cluster binding energies from Jaraiz et al.[31] Interstitial-vacancy interactions from this work.
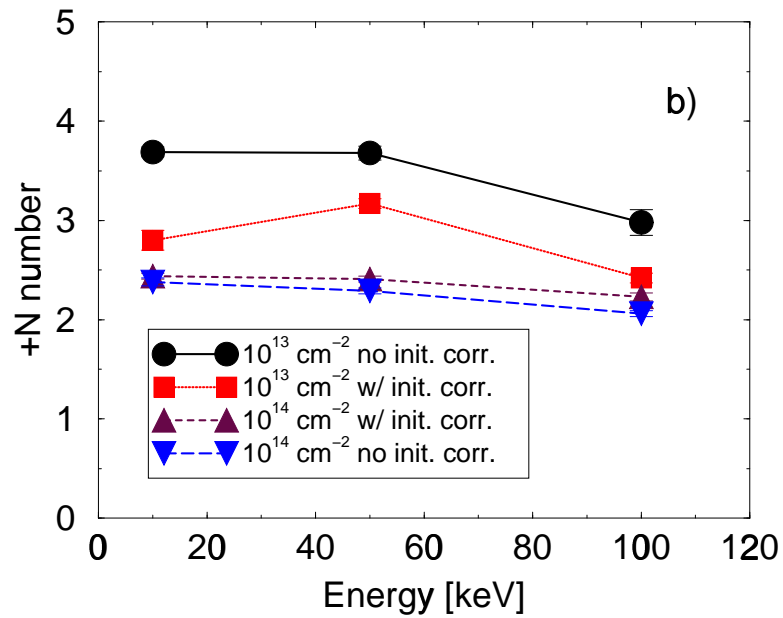
Figure 6.8: +N numbers after vacancies recombine for different doses and energies taking into account long range interaction between an interstitial and a vacancy. Cluster binding energies from Jaraiz et al.[31] Interstitial-vacancy interactions from this work.

range I-V interaction determined from MD was also found to reduce the +N factor.

Chapter 7

Dopant - Defect Interaction

7.1 Boron - Interstitial Interaction

As it was shown in Chapter 2, dopant impurities like B diffuse via an interstitial mechanism. The impurity is converted for short time intervals into a fast migrating intemediate species, dopant interstitial B_i. The relevant reactions for diffusion via B_i are [45]:

$$I + B_s \rightleftharpoons B_i \tag{7.1}$$

$$V + B_i \rightleftharpoons B_s \tag{7.2}$$

$$I + V \rightleftharpoons 0 \tag{7.3}$$

Eq. (7.3) plays an important role by modifying the concentrations of interstitials and vacancies available for reactions (7.1) and (7.2).

The intermitent diffusion is more complicated than the Fickian diffusion. The migration distance has an anomalous temperature dependence:

$$\lambda = \lambda_0 \exp(+E_\lambda/kT) \tag{7.4}$$

where λ_0 is the jump distance between two migration events. Previous calculations[46] showed that reaction (7.1) is exotermic (1.0eV).

This equation implies that as the temperature decreases the dopant migrates for longer distances. Here the Boron interstitial interaction is studied using the ab-initio method discussed in Chapter 3. Besides the use of density functional theory(DFT) and local density approximation (LDA) efficient plane-wave ultrasoft pseudopotential and a 4^3 Monkhorst-Pack k-point sampling are used. The code VASP[47] was used for these calculations. Also a 64 atom supercell is used throughout these calculations. The formation energy of the self-interstitial is defined as:

$$E_f(Si_i) = E(Si_{65}) - \frac{65}{64}E(Si_{64})$$ (7.5)

where $E(Si_{65})$ is the total energy for a 65-atom supercell containing a Si self-interstitial and $E(Si_{64})$ is the total energy for a 64 atom supercell of pure bulk Si.

The formation energy for the Boron substitutional Si self-interstitial pair is defined as:

$$Ef(Bs - Si_i) = E(Si_{64}B) - E(Si_{63}B) - \frac{1}{64}E(Si_{64})$$ (7.6)

Si_i assited B diffusion starts from a bound pair of B and Si_i. The lowest energy is found for a pair with B substitutional and Si_i tetrahedral, see Fig. 7.1a. The binding energy of this pair is 0.9 eV with respect to the more stable dissociation products Si_i^{T+} and B_s^-. A 0.7 eV barrier is found for kiking out Boron from a substitutional position to a hexagonal site (see Fig. 7.1b), which is significantly lower than the 1.1 eV barrier found previously[43]. Then instead of following a hexagonal tetrahedral path as found by Zhu et al.[43], Boron kicks in as Boron substitutional. The energetics for the neutral systems is shown in Fig. 7.2. The activation energy for the diffusion
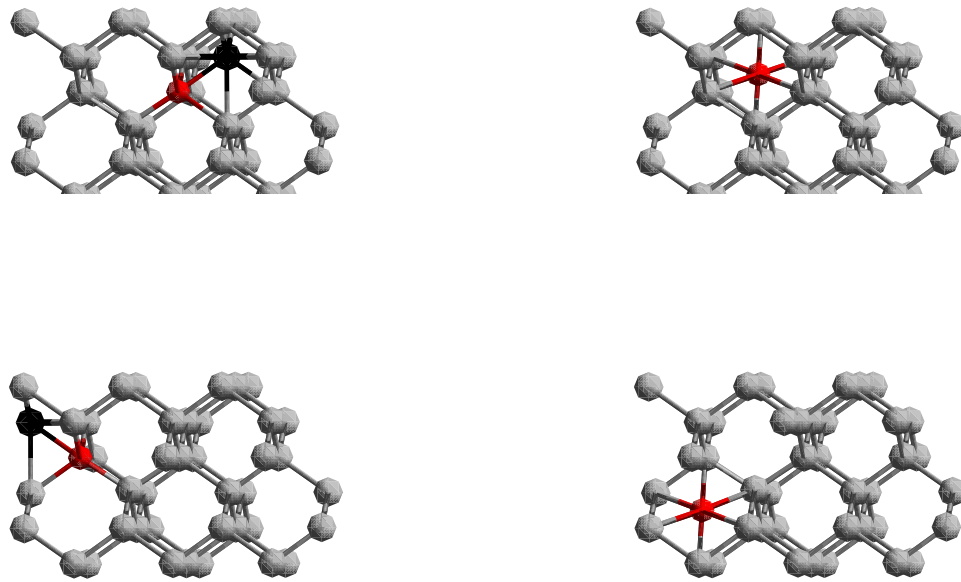
Figure 7.1: Boron diffusion in Si following a substitutional-hexagonal- substitutional path. In a) we have a Boron substitutional Si self interstitial in a tetrahedral position pair, in b) Boron is kicked-out in a hexagonal position becoming interstitial, in c) Boron becomes substitutional again and in d) Boron is kicked-out in another hexagonal position. The migration process ends when the pair dissociates.
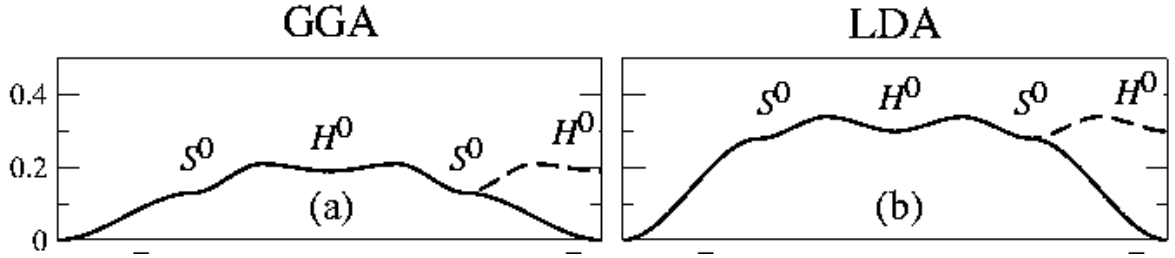
Figure 7.2: The nudged-elastic band total energy (eV) for a neutral system relative to the energy of the initial system of $B - Si_i$ complexes as function of the hyperdistance of the system from the initial configuration. a) within the GGA aproximation, b) within LDA approximation. See Windl *et al.* for complete details.

mechanism described above is given by:

$$Q(B_s) = E_f(B - Si_i) + E_m(B_s) \qquad (7.7)$$

and is found to be 3.0 eV which is the lower bound of the experimental range. This mechanism is also able to explain the anomalous increase in diffusion lenght with decreasing temperature the same way the kick-out mechanism does. As the temperature decreases the Boron substitutional Si interstitial is less likely to dissociate leading to an increase in the diffusion lenght.

Chapter 8

Conclusions

Recent ab-initio calculations have been used to describe the attractive interaction between a dopant and a vacancy in kinetic lattice Monte Carlo calculations of dopant diffusion in a vacancy gradient. It was found that for As the dopant flux driven by a vacancy gradient has the same direction as the vacancy flux with a magnitude that approaches that of ideal pair diffusion at low temperatures (700 C) and drops with increasing temperature. The dopant flux decreases if long range interactions are taken into account. Due to a large exchange barrier which becomes the rate limiting step for pair diffusion, P has a similar behavior but a weaker temperature dependence, leading to dopant fluxes which are smaller at low temperatures, but larger at high temperatures.

Using the vacancy interstitial potential from molecular dynamics calculations the capture radius for Frenkel pair recombination was found to be dependent on the interaction range. At short range interaction it has the value of 3.75 $\AA$. At long range interaction it has the value of 6.5 $\AA$.

The large enhancement in diffusivity at high doping levels is due primarily to collective effects involving the interactions of vacancies with several dopant atoms.

Complexes like As_2V are mobile and contribute significantly to diffusion.

A 50nm nMOS transistor with As doped drain and B doped source was simulated and the evolution in the number of dopant substitutional and dopant interstitial was followed as function of time. A time interval in which B is mostly substitutional was found.The presence of As makes vacancies last longer in the system due to As vacancy clusters. Further work will have to produce faster algorithms. The dependence of energy on clusters size and its influence on the overall system needs also further investigation, since the behavior of these clusters is very sensitive to the energies involved.

Also the initial phases of ion implant annealing were explored in order to predict the resulting effect on transient enhanced diffusion. A factor +N was calculated which is proportional to the number of interstitial remaining after vacancies have recombined. This factor increases at lower doses since faster diffusing vacancies can diffuse to the surface rather than recombining with interstitials. The long range interstitial vacancy interaction determined from MD was also found to reduce the +N factor.

Using ab initio calculations a new mechanism for B diffusion in silicon was found. Rather than a kick out of B into a mobile channel a direct diffusion mechanism for the B interstitial pair was found. The activation energy of 3.5-3.8 eV, migration energy of 0.4-0.7 eV and diffusion lenght exponent of -0.6 - 0.2 eV are in excellent agreement with experiment.

Appendix A

Dopant Diffusion in a Vacancy Gradient

From a phenomenological perspective a dopant (A) interacts with a point defect (V) to form a pair:

$$A + V \Leftrightarrow AV \qquad \text{(A.1)}$$

Mass action law gives the concentration of AV pairs as function of concentration of point defects and dopants:

$$C_{AV} = K_{AV} \cdot C_A \cdot C_V \qquad \text{(A.2)}$$

where K_{AV} is the reaction constant. The dopant flux can then be written as:

$$J_A = J_{AV} = -D_{AV} \cdot \nabla C_{AV} = -D_{AV} \cdot K_{AV} \cdot [C_V \nabla C_A + C_A \nabla C_V] \qquad \text{(A.3)}$$

Kinetic Lattice Monte Carlo (KLMC) predicts a correction γ to the above equation such that the dopant flux can be written now as:

$$J_A = -D_{AV} \cdot K_{AV} \cdot [C_V \nabla C_A + \gamma \cdot C_A \nabla C_V] \qquad (A.4)$$

The numerical implementation of the vacancy gradient is such that there is no dopant gradient. Thus:

$$J_A = -\gamma D_{AV} \cdot K_{AV} \cdot C_A \nabla C_V \qquad (A.5)$$

Isoconcetration experiments performed by Larsen et all. find an effective diffusivity $D^{eff} = D_{AV} \cdot K_{AV} \cdot C_V^*$. With this substitution we obtain:

$$J_A = -\gamma \cdot D_{eff} \cdot C_A \cdot \nabla \frac{C_V}{C_V^*} \qquad (A.6)$$

Effective diffusivity is found by calculating the mean squared displacement of the dopant:

$$D^{eff} = \frac{1}{6 \cdot t} \sum [\Delta \mathbf{r}]^2 \qquad (A.7)$$

where the summation is carried over all dopants present in the simulated system. Introducing the mean displacement $< z >$ and the dopant velocity v we find :

$$v = \frac{J_A}{C_A} = \frac{< z >}{t} = -\gamma \cdot D_{eff} \cdot \nabla \frac{C_V}{C_V^*} \qquad (A.8)$$

From this last relation one finds γ by finding all quantities $v, D^{eff}, \nabla \frac{C_V}{C_V^*}$ numerically.

Bibliography

[1] G. D. Watkins, in *Deep Centers in Semiconductors* edited by S. t. Pantelides (Gordon and Breach, New York, 1986), p. 147.

[2] A. Ural, P.B. Griffin and J.D. Plummer, J. Appl. Phys. **85**, 6440 (1999).

[3] P. M. Fahey, P. B. Griffin, and J. D. Plummer, Rev. Mod. Phys. **61**, 289 (1989).

[4] Hu, S.M., 1974, J. Appl. Phys. **45**, 1567.

[5] O. Pankratov, H. Huang, T. D. de la Rubia and C. Mailhiot, Phys. Rev. B, **56**, 13172 (1997).

[6] J. S. Nelson, P. A. Schultz and A. F. Wright, Appl. Phys. Lett. **73**, 247 (1998).

[7] J. S. Nelson, private communication.

[8] Simmons, R.O., and R. W. Balluffi, Phys. Rev. **117**, 52 (1960).

[9] A. P. Horsefield, S. T. Dunham and H. Fujitani, to be published.

[10] k. Binder and D.W. Heermann, Monte Carlo Simulation in Statistical Physics, Springer Series in Statistical Physics, Edited by Peter Fulde.

[11] R. K. Pathria,Statistical Mechanics 1995.

[12] M. Tang, L. Colombo, J. Zhu and T. Diaz de la Rubia, Phys. Rev B **55**, 14279, (1997).

[13] H. Jonnson, G. Mills and K. W. Jacobsen, H. Jonnsson, G. Mills, K. W. Jacobsen, 'Nudged Elastic Band Method for Finding Minimum Energy Paths of Transitions', in 'Classical and Quantum Dynamics in Condensed Phase Simulations', ed. B. J. Berne, G. Ciccotti and D. F. Coker (World Scientific, 1998), p. 385.

[14] W. Windl, M. M. Bunea, R. Stumpf, S. T. Dunham and M. P. Masquelier, Phys. Rev. Lett. **83**, 4345, 1999.

[15] S. List and H. Ryssel, J. Appl. Phys. **83**, 7585 (1998).

[16] M. Yoshida, J. Appl. Phys. **48**, 2169 (1977).

[17] D. Mathiot and J. C. Pfister, J. Appl. Phys. **55**, 3518 (1984).

[18] K. Maser, Exp. Tech. Phys. **34**, 213 (1986).

[19] M. Kurata, Y. Morikawa, K. Nagami, and H. Kuroda, Jpn. J. Appl. Phys. **12**, 472 (1973).

[20] K. W. Kehr, K. Binder and S. M. Reulein, Phys. Rev. B **39**, 4891 (1989).

[21] L. Onsager, Phys. Rev. **37**,405 (1931); **38**, 2265 (1931).

[22] TSUPREM-4 User's Manual, chapter 2, Release 6.6 (1998).

[23] S.T. Dunham and C.D. Wu., J. Appl. Phys. **78**, 2362 (1995).

[24] S.T. Dunham and C.D. Wu, in *Simulation of Semiconductor Devices and Processes (SISDEP/SISPAD'95)*, edited by H. Ryssel *et al.*, (Springer-Verlag/Wien **6**, 1995), p. 476.

[25] M. M. Bunea and S. T. Dunham, in *Defects and Diffusion in Silicon Processing,* edited by T. Diaz de la Rubia *et al.,* (Mat. Res. Proc. **469**, Pittsburgh, PA 1997), p. 353; Journal of Computer-Aided Materials Design **5**, 81 (1998).

[26] G. H. Vineyard, J. Phys. Chem. Solids **3**, 121 (1957); also as an example for microscopic theories of atomic movements see A. Allnat and A. B. Lidiard, Rep. Prog. Phys. **50**, 373-472 (1987).

[27] E. Chason, S. T. Picraux, J. M. Poate, J. O. Borland, M. I. Current, T. Diaz de la Rubia, D. J. Eaglesham, O. W. Holland, M. E. Law, C. W. Magee, J. W. Mayer, J. MeIngailis, A. F. Tash, J. Appl. Phys. **81**, 6513 (1997).

[28] D. J. Eaglesham, P. A. Stolk, H. J. Gossman and J. M. Poate, Appl. Phys. Lett **65**, 2305 (1994).

[29] M. J. Caturla, M. D. Johnson, T. Diaz de la Rubia, Appl. Phys. Lett **65**, 230 5 (1994).

[30] M. D. Giles, J. Electrochem. Soc. **138**, 1160 (1991).

[31] M. Jaraiz, G. H. Gilmer and J. M. Poate, Appl. Phys. Lett. **68**, 409 (1996).

[32] L. Pelaz, G. H. Gilmer,M. Jaraiz, S. B. Herner, H. J. Gossmann, D. J. Eaglesham, G. Hobler, C. S. Rafferty and J. Barbolla, Appl. Phys. Lett. **73**, 1421 (1998).

[33] M. Z. Bazant and E. Kaxiras, *Phys. Rev. Lett.* **77**, 4370 (1996).

[34] M. Z. Bazant, E. Kaxiras, and J. F. Justo, *Phys. Rev. B* **56**, 8542 (1997).

[35] J. F. Justo, M. Z. Bazant, E. Kaxiras, V. V. Bulatov and S. Yip, Phys. Rev B **58**, 2539, (1998).

[36] B. Obradovic, G. Wang, C. Snell, G. Balamurugan, M. F. Morris, Y. Chen and A. F. Tash, UT-Marlowe User Manual, 1997, Unversity of Texas at Austin.

[37] M. M. Bunea and S. T. Dunham, in Semiconductor Process and Device Performance Modeling, ed. by S. T. Dunham and J. S. Nelson. (Mat. Res. Soc. Proc. **490**, Pittsburgh, PA, 1998) pp. 3-8.

[38] M. Ramamoorthy and S. T. Pantelides, Phys. Rev. Lett. **76**, 4753 (1996).

[39] S. M. Hu, Phys. Status. Solidi. **B60**, 595 (1973).

[40] A.N. Larsen, K.K. Larsen and P.E. Andersen, J. Appl. Phys. **73**, 691 (1993).

[41] R. B. Fair and G. R. Weber, J. Appl. Phys. **44**, 273 (1973).

[42] The National Technology Roadmap for Semiconductors (Semiconductor Industry Association, 1997)

[43] J. Zhu, T. Diaz de la Rubia, L. H. Yang, C. Mailhiot, and G. H. Gilmer, Phys. rev. B **54**, 4741 (1996)

[44] G. D. Watkins, J. R. Troxell and A. P. Chatterjee, in *Defects and Radiation Effects in Semiconductors*, edited by J. H. Albany (Institute of Physics Conference Series No. 46, 1979) p. 16

[45] N. E. B. Cowern, G. F. A. van de Walle, P. C. Zalm, and D. J. Oostra, Phys. Rev. Lett. bf 69, 116 (1992).

[46] N. E. B. Cowern, G. F. A. van de Walle, D. J. Gravesteijn, and C. J. Vriezema, Phys. Rev. Lett. **67**, 212 (1991).

[47] VASP manual, chapter 8.6 (http://tph.tuwien.ac.at/ ∼vasp/guide/vasp.html).

[48] M.M. Bunea, P. Fastenko and S.T. Dunham. in Silicon Front-End Processing-Physics and Technology of Dopant-Defect Technology, H-J. L. Gossmann,T.E. Haynes, M.E. Law, A.N. Larsen, S. Odanaka eds. (Mat. Res. Soc. Proc. 568, Pittsburgh, PA, 1999 Spring Meeting), p. 135.